Metabolic Engineering 62 (2020) 260–274

Contents lists available at ScienceDirect

Metabolic Engineering

journal homepage: www.elsevier.com/locate/meteng

Original Research Article

Gene amplification, laboratory evolution, and biosensor screening reveal MucK as a terephthalic acid transporter in *Acinetobacter baylyi* ADP1

Isabel Pardo [a,b,1], Ramesh K. Jha [b,c,1], Ryan E. Bermel [b,c], Felicia Bratti [a,b], Molly Gaddis [a,b], Emily McIntyre [d], William Michener [a,b], Ellen L. Neidle [d], Taraka Dale [b,c], Gregg T. Beckham [a,b,**], Christopher W. Johnson [a,b,*]

[a] Renewable Resources and Enabling Sciences Center, National Renewable Energy Laboratory, Golden CO, USA
[b] Agile BioFoundry, Emeryville CA, USA
[c] Bioscience Division, Los Alamos National Laboratory, Los Alamos NM, USA
[d] Department of Microbiology, University of Georgia, Athens GA, USA

ARTICLE INFO

Keywords:
Adaptive laboratory evolution
Major facilitator superfamily transporter
mucK
Acinetobacter baylyi ADP1
Plastics upcycling
Plastics bioconversion
TPA biosensor

ABSTRACT

Microbial terephthalic acid (TPA) catabolic pathways are conserved among the few bacteria known to turnover this xenobiotic aromatic compound. However, to date there are few reported cases in which this pathway has been successfully expressed in heterologous hosts to impart efficient utilization of TPA as a sole carbon source. In this work, we aimed to engineer TPA conversion in *Acinetobacter baylyi* ADP1 via the heterologous expression of catabolic and transporter genes from a native TPA-utilizing bacterium. Specifically, we obtained ADP1-derived strains capable of growing on TPA as the sole carbon source using chromosomal insertion and targeted amplification of the *tph* catabolic operon from *Comamonas* sp. E6. Adaptive laboratory evolution was then used to improve growth on this substrate. TPA consumption rates of the evolved strains, which retained multiple copies of the *tph* genes, were ~0.2 g/L/h (or ~1 g TPA/g cells/h), similar to that of *Comamonas* sp. E6 and almost 2-fold higher than that of *Rhodococcus jostii* RHA1, another native TPA-utilizing strain. To evaluate TPA transport in the evolved ADP1 strains, we engineered a TPA biosensor consisting of the transcription factor TphR and a fluorescent reporter. In combination with whole-genome sequencing, the TPA biosensor revealed that transport of TPA was not mediated by the heterologous proteins from *Comamonas* sp. E6. Instead, the endogenous ADP1 muconate transporter MucK, a member of the major facilitator superfamily, was responsible for TPA transport in several evolved strains in which MucK variants were found to enhance TPA uptake. Furthermore, the IclR-type transcriptional regulator DcaS was identified as a repressor of *mucK* expression. Overall, this work presents an unexpected function of a native protein identified through gene amplification, adaptive laboratory evolution, and a combination of screening methods. This study also provides a TPA biosensor for application in ADP1 and identifies transporter variants for use in metabolic engineering applications focused on plastic upcycling of polyesters.

1. Introduction

Terephthalic acid (TPA) is a commodity chemical for which worldwide consumption in 2018 was >65 million metric tons (IHS Markit, 2019). TPA is most commonly used in the ubiquitous polyester, polyethylene terephthalate (PET), a synthetic polymer generally employed in the production of fibers (~60% of total TPA market), single-use beverage bottles, and packaging. Despite being the most widely recycled plastic, the majority of used PET is discarded, ending up in landfills or leaking to the environment (NAPCOR Report, 2018). Currently, most PET recycling consists of mechanical approaches, which result in down-cycling to products of lesser value due to the loss of polymer properties with each reprocessing cycle (Rahimi and García, 2017). Therefore, there is growing interest in the deconstruction of PET into its

* Corresponding author. Renewable Resources and Enabling Sciences Center, National Renewable Energy Laboratory, Golden CO, USA.
** Corresponding author. Agile BioFoundry, Emeryville CA, USA.
E-mail addresses: gregg.beckham@nrel.gov (G.T. Beckham), christopher.johnson@nrel.gov (C.W. Johnson).
[1] Denotes equal contribution.

https://doi.org/10.1016/j.ymben.2020.09.009
Received 11 May 2020; Received in revised form 11 September 2020; Accepted 19 September 2020
Available online 1 October 2020

constituent monomers TPA and ethylene glycol, or other processable intermediates, for their subsequent repolymerization or conversion into new materials (Kenny et al., 2012, 2008; Rorrer et al., 2019; Wierckx et al., 2015). Known PET chemical recycling methods include catalytic processes such as glycolysis, methanolysis, or hydrolysis (Garcia and Robertson, 2017; Sinha et al., 2010). Similarly, the biological depolymerization of PET to TPA and ethylene glycol can be mediated by hydrolytic enzymes (Herrero Acero et al., 2011; Müller et al., 2005; Ribitsch et al., 2012; Ronkvist et al., 2009; Sulaiman et al., 2012; Yoshida et al., 2016). In this context, the combination of PET chemical recycling with the biological assimilation of released monomers has gained significant attention, as this technology could enable use of this waste plastic as feedstock for the microbial conversion into value-added products.

Bacterial pathways for the catabolism of ethylene glycol (Franden et al., 2018; Li et al., 2019; Mückschel et al., 2012) and TPA are known, although not comprehensively studied to date. In particular, the genes responsible for converting TPA to protocatechuate (PCA), a common intermediate in aromatic catabolic pathways, are reported in the literature for only a few bacteria, including several species of *Comamonas* (Sasoh et al., 2006; Wang et al., 1995) and *Rhodococcus* (Choi et al., 2005; Patrauchan et al., 2005), *Paraburkholderia xenovorans* (formerly *Burkholderia xenovorans*, Chain et al., 2006), *Delftia tsuhuratensis* (Shigematsu et al., 2003), and *Ideonella sakaiensis* (Yoshida et al., 2016). Genome mining studies have also identified other potential TPA-utilizing bacteria (Salvador et al., 2019). In these bacteria, TPA is first converted by a three-component TPA 1,2-dioxygenase (TPADO) into a non-aromatic *cis*-dihydrodiol compound. Subsequently, this product is decarboxylated by a dehydrogenase to PCA, a common substrate for ring cleavage through which bacteria typically funnel diverse aromatic compounds such as those derived from lignin into central metabolism (Fuchs et al., 2011; Linger et al., 2014).Whereas the genes responsible for TPA conversion to PCA and their organization within the operon are surprisingly conserved in the known catabolic pathway to date, bacteria have been reported to employ two different mechanisms for TPA import. In *Comamonas* sp. And *I. sakaiensis,* TPA is imported by a tripartite tricarboxylate transporter (TTT), composed of a periplasmic substrate binding protein (SBP) and two transmembrane proteins. While the gene encoding the SBP is found upstream of the TPA catabolic genes within the operon, genes coding for transmembrane proteins are located elsewhere in the chromosome (Hosaka et al., 2013; Yoshida et al., 2016). Conversely, *Rhodococcus* sp. and *P. xenovorans* exhibit genes coding for major facilitator superfamily (MFS) transporters downstream of the catabolic genes within the operon (Chain et al., 2006; Choi et al., 2005; Patrauchan et al., 2005).

Given that it is a dicarboxylic acid, TPA likely cannot readily diffuse through the cell membrane at neutral pH (Vermaas et al., 2019). Therefore, the expression of TPA transporter genes is expected to be essential to enable TPA catabolism in heterologous hosts. To date, the only reported example of an engineered microorganism that grows on TPA as a sole carbon source was obtained by expressing the SBP and catabolic genes from *Comamonas* sp. E6 in a closely related *Comamonas testosteroni* strain (Sasoh et al., 2006). However, growth on TPA was not conferred in a more distant *Pseudomonas putida* strain by the expression of both the TTT and catabolic genes from *Comamonas* sp. E6, although such expression was sufficient for TPA uptake and conversion (Hosaka et al., 2013).

In this work, we aimed to engineer and evolve *Acinetobacter baylyi* ADP1 (wild-type strain hereafter referred to as ADP1) for rapid transport and consumption of TPA using the Evolution by Amplification and Synthetic biology (EASy) method (Tumen-Velasquez et al., 2018). EASy allows the amplification of defined segments in the chromosome and has been previously used to evolve engineered strains in which expression of heterologous genes, in single copy, were insufficient to support growth on a non-native substrate. First, genes encoding the TPA transporter and catabolic proteins from *Comomonas* sp. E6 were chromosomally inserted in ADP1. Next, gene dosage of the catabolic genes was increased with EASy, and, following adaptive laboratory evolution (ALE), whole-genome sequencing (WGS) was used to identify mutations in evolved isolates (Dragosits and Mattanovich, 2013; Portnoy et al., 2011; Sandberg et al., 2019). The results indicated that MucK, a native MFS transporter known to import muconate in ADP1 (Williams and Shaw, 1997), could be responsible for TPA uptake in several evolved isolates. To examine this possibility, we engineered a transcription factor-based TPA biosensor coupled to a fluorescent reporter to evaluate TPA import. The biosensor confirmed that MucK was indeed capable of transporting TPA, and further identified MucK variants that were more efficient in TPA uptake. Finally, the regulation of MucK expression by a previously uncharacterized transcription factor, DcaS, was also elucidated.

2. Materials and methods

2.1. Strains and culture media

A. baylyi ADP1 (American Type Culture Collection ATCC 33305) and derived strains were routinely grown aerobically at 30 °C in minimal medium (MM) (Shanley et al., 1986), consisting of 0.5 M KH_2PO_4, 0.5 M Na_2HPO_4, 10% $(NH_4)_2SO_4$, and 1 mL concentrated base solution. Concentrated base solution contained (per liter): 20 g nitriloacetic acid (dissolved in 600 mL H_2O with 14.6 g KOH); 28.9 g $MgSO_4$; 6.67 g $CaCl_2{\cdot}2H_2O$; 18.5 mg $Mo_7O_{24}{\cdot}4H_2O$; 198 mg $FeSO_4{\cdot}7H_2O$; and 100 mL of Metals 44 solution. The Metals 44 solution contained (per liter): 2.5 g EDTA; 10.95 g $ZnSO_4{\cdot}7H_2O$; 5 g $FeSO_4{\cdot}7H_2O$; 1.54 g $MnSO_4{\cdot}7H_2O$; 392 mg $CuSO_4{\cdot}5H_2O$; 250 mg $Co(NO_3)_2{\cdot}6H_2O$; and 177 mg $Na_2B_4O_7{\cdot}10H_2O$. Minimal medium was supplemented with 20 mM pyruvate (hereafter MMP) or 5 or 10 mM TPA as carbon sources, unless otherwise indicated. For growth on plates, 1.5% w/v agar was added. When noted, the media was adjusted to pH 6 by changing the ratio of phosphate salts. *Comamonas* sp. E6 (Biological Resource Center, NITE, strain number 107749) and *Rhodococcus jostii* RHA1 (kindly provided by Dr. Lindsay Eltis from the University of British Columbia) were grown in lysogeny broth (LB) or MM supplemented with 10 mM TPA. *Escherichia coli* NEB 5-alpha F'I^q and NEB 5-alpha cells (New England Biolabs) were grown in LB broth. Antibiotic concentrations used for ADP1 were 25 μg/mL (standard) or 1 mg/mL (high) kanamycin (Km), and 25 μg/mL streptomycin (Sm). For *E. coli*, 100 μg/mL ampicillin (Ap), and 50 μg/mL Km or Sm were used.

2.2. Plasmid construction

Routine PCR amplifications were carried out using Phusion High-Fidelity DNA polymerase (New England Biolabs) and primers synthesized by Integrated DNA Technologies (IDT) or Eurofins. Synthetic, double-stranded DNA fragments (gBlocks) were also synthesized by IDT. Plasmids were constructed either by NEBuilder HiFi DNA assembly or by ligation with T4 DNA ligase (both from New England Biolabs). Plasmids containing P_{tac} were transformed and maintained in NEB 5-alpha F'I^q cells. All plasmid inserts were verified by Sanger sequencing, performed by GENEWIZ. Details on plasmid construction and primer and gBlock sequences can be found in Supplementary Tables 1–3.

2.3. Strain construction

Chromosomal modifications were engineered in *A. baylyi* by natural transformation of recipient strains with linear DNA fragments (Biggs et al., 2020). These DNA fragments were obtained by PCR or from restriction enzyme digestion of plasmids. To increase transformation efficiency, cells were grown in MMP instead of LB broth. To facilitate efficient homologous recombination, the transforming DNA carried 1–2 kbp of sequence that was identical to the chromosomal target on each side of the mutated region (de Berardinis et al., 2008; Metzgar et al., 2004). *A. baylyi* mutants were selected on MMP plates with the

appropriate antibiotic, or on YT+25% sucrose (10 g/L yeast extract, 20 g/L tryptone, 250 g/L sucrose, and 18 g/L agar) in the case of *sacB* counterselection (Johnson and Beckham, 2015). Genotypes were confirmed by colony PCR with MyTaq HS Red Mix (Bioline) and, in some cases, Sanger sequencing of localized regions. A brief description of the strains used in this study is provided in Table 1 and Fig. 1. Details on strain construction can be found in Supplementary Table 4.

Table 1
Description of *A. baylyi* strains, isolates, and lineages used in this work. For the purpose of standardized nomenclature, *tphA* genes are numbered in subscript to differentiate them from mutated alleles. More details on the genotype and strain construction can be found in Supplementary Table 4.

Strains, isolates, and lineages	Relevant features
Strains	
ADP1	Wild type
IP115	*pobA*:P_{tac}:*tphCA*$_2$*A*$_3$*BA*$_1$:ΩKm^R
IP130	*pobA*:P_{tac}:*tphCA*$_2$*A*$_3$*BA*$_1$:*tpiBA*:ΩKm^R
IP148	*pobA*:P_{tac}:*tphCA*$_2$*A*$_3$*BA*$_1$:ΩKm^R:P_{trc}:*tpiBA1481*:*tpiA1482* [*tpiA1481* encodes TpiA(W366*); *tpiA1482* encodes TpiA (Δ1–370)]
IP297	*pobA*:P_{tac}:*tphC*:ΩKm^R:P_{trc}:*tpiBA1481*
IP313	*pobA*:P_{tac}:*tphC*:ΩKm^R:P_{trc}:*tpiBA*
IP337	*pobA*:P_{tac}:*tphC*:ΩKm^R:P_{trc}:*tpiBA1481*:*tphA1482* (obtained by deletion of *tphA*$_2$*A*$_3$*BA*$_1$ genes in IP148)
IP348	*pobA*:P_{tac}:*tphC*:ΩKm^R:P_{trc}:*tpiBA1481*:*tphA1482* (obtained by *de novo* integration in ADP1)
IP367	IP148-derived mutant, Δ*mucK*::Sm^R:*sacB*
IP378	IP148-derived mutant, Δ*dcaS*
IP387	IP148-derived mutant, Δ*dcaS* Δ*mucK*::Sm^R:*sacB*
IP398	IP148-derived mutant, Δ*mucK*::*mucK258* [encodes MucK (M34I E53G)]
IP400	IP148-derived mutant, Δ*mucK*::*mucK243* [encodes MucK (M34L T342I)]
IP402	IP148-derived mutant, Δ*mucK*::*mucK255* [encodes MucK (W150C I403T)]
IP411	IP148-derived mutant, Δ*mucK*::*mucK246* [encodes MucK (Y133C)]
IP413	IP148-derived mutant, Δ*dcaS* Δ*mucK*::*mucK258*
IP415	IP148-derived mutant, Δ*dcaS* Δ*mucK*::*mucK243*
IP417	IP148-derived mutant, Δ*dcaS* Δ*mucK*::*mucK255*
IP419	IP148-derived mutant, Δ*dcaS* Δ*mucK*::*mucK246*
IP461	ADP1-derived mutant, Δ*dcaS*
IP492	ADP1-derived mutant, Δ*mucK*::*mucK258*
IP493	ADP1-derived mutant, Δ*mucK*::*mucK243*
IP494	ADP1-derived mutant, Δ*mucK*::*mucK255*
IP495	ADP1-derived mutant, Δ*mucK*::*mucK246*
IP496	ADP1-derived mutant, Δ*dcaS* Δ*mucK*::*mucK258*
IP497	ADP1-derived mutant, Δ*dcaS* Δ*mucK*::*mucK243*
IP498	ADP1-derived mutant, Δ*dcaS* Δ*mucK*::*mucK255*
IP499	ADP1-derived mutant, Δ*dcaS* Δ*mucK*::*mucK246*
Tpa$^+$ isolates and ALE lineages (multiple copies of *tph* genes)	
TPA_1	IP148-derived isolate, used to initiate ALE
TPA_2	IP148-derived isolate, used to initiate ALE
TPA_3	IP148-derived isolate, used to initiate ALE
TPA_4	IP148-derived isolate, used to initiate ALE
TPA_1.6	ALE lineage derived from TPA_1, evolved at pH 6
TPA_1.7	ALE lineage derived from TPA_1, evolved at pH 7
TPA_2.6	ALE lineage derived from TPA_2, evolved at pH 6
TPA_2.7	ALE lineage derived from TPA_2, evolved at pH 7
TPA_3.6	ALE lineage derived from TPA_3, evolved at pH 6
TPA_3.7	ALE lineage derived from TPA_3, evolved at pH 7
TPA_4.6	ALE lineage derived from TPA_4, evolved at pH 6
TPA_4.7	ALE lineage derived from TPA_4, evolved at pH 7
IP243	Isolate from lineage TPA_1.6 after ~750 generations
IP246	Isolate from lineage TPA_1.7 after ~750 generations
IP247	Isolate from lineage TPA_2.6 after ~750 generations
IP250	Isolate from lineage TPA_2.7 after ~750 generations
IP251	Isolate from lineage TPA_3.6 after ~750 generations
IP254	Isolate from lineage TPA_3.7 after ~750 generations
IP255	Isolate from lineage TPA_4.6 after ~750 generations
IP258	Isolate from lineage TPA_4.7 after ~750 generations

2.4. Chromosomal gene amplification and adaptive laboratory evolution by EASy

Chromosomal amplification was achieved by natural transformation of IP148 with a synthetic bridging fragment (SBF) and selecting on high-Km (Tumen-Velasquez et al., 2018). The SBF defines the chromosomal region to be amplified and promotes duplication and further amplification through homologous recombination. For the construction of a SBF, the first and last ~1000 bp of the synthetic P_{tac}:*tphCA2A3BA1*:ΩKm^R cassette were amplified by PCR and fused tail-to-head by overlap extension PCR (see Supplementary materials and methods). The resulting ~2 kbp SBF was transformed into strain IP148 and mutants with increased gene copy number were selected on MMP plates supplemented with 1 mg/mL Km. Growth on high-Km is presumably due to multiple copies of the Km^R gene, resulting from the chromosomal amplification of a region encompassing it. This region (the amplicon) also encompasses the genes needed for TPA consumption. Individual colonies confirmed by colony PCR to have integrated the SBF were re-streaked on a new high-Km plate and grown at 30 °C. By scraping cells from the high-Km plate and streaking on a MM plate with 5 mM TPA as the carbon source (and no antibiotic pressure), selection for optimal copy number of the tandemly arrayed amplicon is altered, and changes in gene dosage can thereby enable the new phenotype, *i.e.* growth on TPA (Tpa$^+$). In this fashion, four Tpa$^+$ colony isolates, designated TPA_1 to TPA_4, were selected and confirmed to contain the SBF by colony PCR.

After growth on a second TPA plate, each isolate was used in adaptive laboratory evolution (ALE) conducted by serial transfer in MM with 5 or 10 mM TPA as the carbon source. Each isolate was evolved at pH 6 and pH 7 in parallel (8 lineages in total). Two-mL cultures (in 13 mm test tubes) were grown at 30 °C with shaking (225 rpm). When cultures reached stationary phase, cells were diluted 100 or 200-fold in 2 mL of fresh medium. Weekly, glycerol stocks were prepared, and genomic DNA from each culture was extracted with the Quick-DNA Miniprep Plus kit (Zymo Research) for quantitation of the average gene copy number.

2.5. Gene copy number analysis by quantitative PCR

Quantitative PCR (qPCR) was carried out using 6FAM-MGBNFQ labelled TaqMan probes and TaqMan Gene Expression Master Mix (Thermo Scientific) in a Bio-Rad CFX96 thermocycler. Primer and probe sequences are provided in Supplementary Table 5. To evaluate changes in amplicon copy number during ALE, relative amounts of the Km^R gene were calculated with respect to *rpoA*, as previously described (Tumen-Velasquez et al., 2018). For spontaneous amplification mutants not obtained by transformation with the SBF, primers and a probe specific for the synthetic *tphA*$_2$ gene were used. All reactions were carried out with four technical replicates per genomic DNA sample, with single-copy parent strain IP148 included as control.

2.6. Whole-genome sequencing and variant analysis

After ~750 generations of ALE, cells from each individual lineage were diluted 10^7-fold and 100 μL plated on MM agar with 5 mM TPA. Two individual colonies from each lineage were selected and the amplicon copy number verified by qPCR. The clone with the lowest copy number from each linage was selected for whole-genome sequencing and phenotypic characterization. Approximately 1 μg of genomic DNA was fragmented by sonication to an average size of 300–500 bp. End repair, A-tailing, and adapter ligation reactions were performed on the fragmented DNA using the NEBNext Ultra II kit (New England Biolabs). Illumina paired-end sequencing was performed on a NextSeq500 device at the Georgia Genomics Facility (University of Georgia). Sequence analysis and variant calling (minimal frequency set at 0.25) was performed with Geneious Prime software against the theoretical genome sequence of IP148 parent strain and a modified sequence presenting two

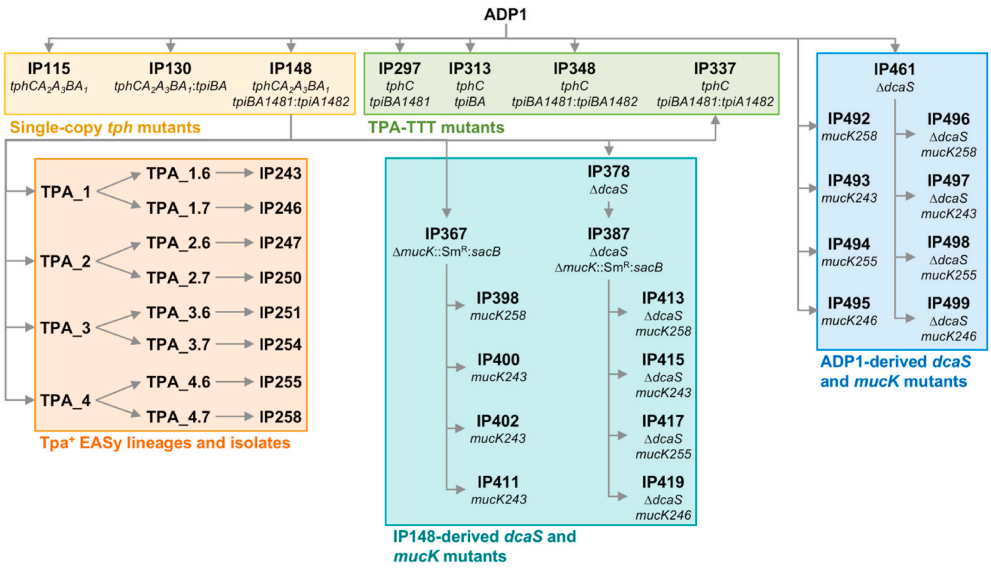

Fig. 1. Dendrogram of *A. baylyi* strains and isolates used in this work. Mutations introduced during strain construction relevant to TPA catabolism and transport are indicated.

copies of the amplicon (partial sequences provided in Supplementary Files 1 and 2). The wild-type ADP1 genome sequence (National Center for Biotechnology Information accession number NC_005966) was used as reference.

2.7. Evaluation of growth and TPA consumption by cultures grown in microtiter plates and shake-flasks

To evaluate growth of *A. baylyi* mutants, cultures in microtiter plates were analyzed with a Bioscreen C MBR plate-reader (Growth Curves USA). Cells for inoculation were grown overnight in MMP at 30 °C and 225 rpm. After collection by centrifugation, cells were washed with MM (no carbon source) and added to 300 µL media to an OD_{600} of 0.05 (per well). Cells were incubated at 30 °C with shaking and $OD_{420\text{-}580}$ measured at 15-min intervals.

For shake-flask cultures, cells for inoculation were grown overnight in MMP (*A. baylyi*) or LB broth (*Comamonas* sp. E6 and *R. jostii* RHA1) at 30 °C and 225 rpm. After collection by centrifugation, cells were washed with MM (no carbon source). For wild-type ADP1 and single-copy mutants, cells were inoculated to an OD_{600} of 0.02 in 25 mL MMP supplemented with 5 mM TPA (pH 6 and 7) in 125-mL flasks. For Tpa^+ *A. baylyi* mutants, *Comamonas* sp. E6, and *R. jostii* RHA1, cells were inoculated to an OD_{600} of 0.02 in 50 mL MM with 10 mM TPA (pH 6 or 7) in 250-mL flasks. In all cases, cells were grown at 30 °C, 225 rpm, and sampled regularly by removing 1 mL aliquots for OD_{600} measurements and HPLC analysis. Standard curves were made to correlate cell dry weight to OD_{600} for strains *A. baylyi* IP148, *Comamonas* sp. E6, and *R. jostii* RHA1. More detail is provided in the Supplementary materials and methods.

2.8. HPLC analysis

HPLC analysis of samples was performed on an Agilent 1260 LC system (Agilent Technologies) equipped with a G7117C diode array detector (DAD). All samples and standards were injected at a volume of 10 µL onto a Phenomenex Luna C18(2), 5 µm, 4.6 × 150 mm column. The column temperature was maintained at 30 °C and the buffers used to separate the analytes of interest were (A) 20 mM phosphate buffer in water and (B) methanol. The separation was carried out using a gradient program of: (A) = 80% and (B) = 20% at time t = 0; (A) = 35% and (B) = 65% at time t = 15 min; and (A) = 80% and (B) = 20% at t = 15.01 min through 20 min. The flow rate was held constant at 0.6 mL/min for a total run time of 20 min. DAD wavelength of 240 nm was used for analysis of TPA while pyruvic acid signal was collected at 210 nm. Calibration curve concentration for each analyte varied between the ranges of 0.1–2500 µg/L. A minimum of 5–6 calibration levels was used with an R^2 coefficient of 0.995 or better for each analyte. A check calibration standard was analyzed every 10–20 samples to ensure the integrity of the initial calibration.

2.9. Building plasmid libraries encoding TPA sensors

The sensor plasmids were constructed using a modified pBAV1K backbone (Addgene plasmid #26702; Bryksin and Matsumura, 2010) in which Km^R was replaced with Sm^R, as described in Supplementary Table 1 for pIP055. The *tphR* coding sequence and the intergenic *tphR-tphC* regulatory region from *Comamonas testosteroni* (American Type Culture Collection strain number 700441D-5), together with the superfolder green fluorescent protein (sfGFP) gene (Pédelacq et al., 2006), were assembled into the vector backbone by NEBuilder HiFi DNA assembly. Targeted diversification in different sites of the *tphR-tphC* regulatory region was achieved by PCR amplification with primers randomized at specific positions. PCR products, along with the genes coding for TphR and sfGFP, were assembled into the vector backbone. Following assembly, the mix was purified using a QIAGEN PCR clean up kit and transformed into electrocompetent NEB 5-alpha cells. The transformants were grown on LB + Sm agar at 37 °C, pooled, and used for plasmid DNA extraction with a commercial kit. The extracted DNA was used for transformation into *A. baylyi*.

2.10. Transformation of biosensor plasmid libraries into A. baylyi

For the transformation of biosensor plasmid libraries, the natural transformation protocol (Biggs et al., 2020) was used, with slight modifications. *A. baylyi* cultures were started from glycerol stocks in 1 mL MMP and grown overnight at 30 °C under constant shaking. A small volume of the overnight culture (70 µL) was then added to 1 mL fresh MMP and mixed with ~100 ng of plasmid DNA. The cells were incubated at 30 °C under constant shaking for 2–6 h, spun down at 5000 rpm for 3 min in a tabletop centrifuge at ambient temperature, and the concentrated pellet plated on MMP + Sm. In order to cover a large library diversity, overnight cells were concentrated 10-fold. Then, 70 µL of the concentrated cells were mixed with up to 300 ng of plasmid DNA in 1 mL MMP and incubated as described above. Multiple parallel transformations were carried out for larger libraries. Plates were

incubated overnight at 30 °C. Colonies from plates were then scraped and resuspended in 2 mL of liquid media, rotated gently for 15 min for homogeneity, and subsequently saved as glycerol stocks.

2.11. Flow cytometry and cell sorting

A. baylyi mutants transformed with biosensor plasmid libraries were pooled by scraping from plates and diluted to an OD_{600} of ~0.05. After growth for 2–4 h, TPA was added at various concentrations (in the range of 0–3 mM) to induce expression of the sfGFP gene. The cultures were grown overnight at 30 °C and analyzed by fluorescence-activated cell sorting (FACS) on a FACSAria III flow cytometer (BD Biosciences), using the standard settings for GFP fluorescence (488 nm excitation laser and 530/30 nm bandpass emission filter). The cells were gated based on forward and side light scatter (FSC/SSC). Based on the theoretical diversity of the libraries, two to three rounds of sorting were performed. These rounds consisted of positive (top 1–3% fluorescent cells from an induced population) and negative (bottom 50–80% low fluorescent cells from an uninduced population) cell sorting. In any round of sorting, 25–50 thousand cells were collected. Finally, the sorted cells were grown on MMP + Sm plates and colonies picked for individual clone verification.

Individual colonies were inoculated into 600 μL of MMP in a 96 deep-well v-bottom plate (Agilent) and grown for 6 h at 30 °C and 1000 rpm in a deep-well maximizer shaker (Taitec Bioshaker MBR-022UP). The cultures were then split into replicate wells, after which one of the two sets was provided with 0.3 mM TPA to induce expression of the sfGFP gene. After overnight growth, cells were diluted 20- to 50-fold in phosphate buffer saline (PBS) and analyzed on an Accuri C6 flow cytometer (BD Biosciences) under the standard settings for GFP measurements (excitation 488 nm and emission 533/30 nm). The cells were gated based on FSC/SSC, and the clones with the highest contrast ratios (induced/uninduced fluorescence response) were selected for further evaluation.

2.12. Dose response and specificity testing of the TPA sensor

A. baylyi mutants were transformed with selected plasmids and grown on MMP + Sm plates. Three colonies were picked and grown overnight as seed cultures. These cultures were diluted 50-fold into 10 mL MMP + Sm and grown for 2–4 h in a 50-mL conical tube to an OD_{600} of ~0.6. The culture was then split into triplicate wells in a 96 deep-well v-bottom plate. Into each well (containing 270 μL of culture), 30 μL of 10x stock solutions of possible inducers of sfGFP gene expression were added (in the range of 0–100 mM for each). Cultures were grown overnight and analyzed using an Accuri C6 flow cytometer (BD Biosciences), following the protocol described above.

2.13. Evaluation of TPA transport in A. baylyi with the TPA sensor

A. baylyi mutants were naturally transformed with plasmids encoding the TPA biosensors. After selection on MMP + Sm plates, transformants were grown overnight in the same medium at 30 °C with shaking, collected by centrifugation, and washed with MM. Cells were then used to inoculate, to an OD_{600} of 0.05, 200 μL of medium per well of 96-well black, clear flat-bottom plates (Corning). Cultures contained MMP + Sm with varied concentrations of TPA. Plates were incubated at 30 °C with shaking in an Infinite®F500 Tecan plate reader for 24 h. The OD_{600} and fluorescence at 520 nm (excitation at 488 nm) were measured at 15-min intervals. The gain used for fluorescence reads was adjusted manually.

2.14. Gene expression analysis by reverse transcriptase-quantitative PCR (RT-qPCR)

Wild-type ADP1 and Δ*dcaS* mutant IP461 were grown overnight in MMP at 30 °C, 225 rpm. Cells were harvested by centrifugation, washed with MM, and inoculated in triplicate to an OD_{600} of 0.1 in 25 mL MM with either 20 mM pyruvate, 5 mM muconate, or 5 mM PCA as the carbon source, in 125-mL flasks. Cells were grown at 30 °C, 225 rpm, to an OD_{600} of ~0.6, after which cells were harvested by centrifugation, flash-frozen in liquid nitrogen, and stored at -80 °C. For RNA extraction, cells were lysed by bead-beating and RNA purified with a QIAGEN RNeasy Mini kit. Genomic DNA was digested with a TURBO DNA-free kit (Thermo Scientific) and cDNA was synthesized with iScript Reverse Transcription Supermix using random primers (Bio-Rad). qPCR was performed in triplicate for each biological sample with 6FAM-MGBNFQ labelled TaqMan probes and TaqMan Gene Expression Master Mix (Thermo Scientific). Primer and probe sequences are provided in Supplementary Table 5. Expression of *mucK* relative to *rpoA* was calculated using the $2^{-\Delta\Delta Ct}$ method (Livak and Schmittgen, 2001).

3. Results

3.1. Heterologous expression of genes encoding TPA transport and catabolism in ADP1

To confer growth on TPA, we introduced genes needed to convert this substrate to PCA, a metabolite that is consumed via the native β-ketoadipate pathway, into ADP1 (Fig. 2A, B). The first step of this conversion, *i.e.* the hydroxylation of the aromatic ring, is catalyzed by TPADO. This multicomponent enzyme consists of a two-subunit Rieske non-heme iron oxygenase, encoded by $tphA_2$ and $tphA_3$, and a multidomain reductase component, encoded by $tphA_1$. The second step in forming PCA is catalyzed by a diol dehydrogenase, encoded by *tphB*. Furthermore, we predicted that growth on TPA would require a transporter. For this purpose, we also introduced the genes coding for the TPA-TTT, consisting of a periplasmic substrate binding protein, encoded by *tphC*, and two cytoplasmic transmembrane proteins, encoded by *tpiA* and *tpiB*. In *Comamonas* sp. E6, all the *tph* genes are organized in an operon, whereas *tpiBA* form a distinct transcriptional unit. Here, the *Comamonas* genes of the tph_{II} operon and the *tpiBA* genes were codon optimized for expression in ADP1 and synthesized as a polycistronic DNA cassette (Fig. 2B).

Initially, high expression of all genes was targeted by replacing the native promoter with a constitutive *tac* promoter (P_{tac}) and by inserting synthetic ribosome binding site (RBS) sequences with high predicted translation initiation rates (TIR, ~10,000 arbitrary units, a.u.) (www.denovodna.com; Espah Borujeni et al., 2014; Salis et al., 2009). However, attempts to integrate this large cassette into the ADP1 chromosome were unsuccessful. This fragment had 9 kbp of synthetic sequence, flanked on either side by 2 kbp of DNA identical to the chromosomal target for integration downstream of *pobA*. To reduce the size of the transforming DNA, the synthetic cassette was split into three fragments for use in a stepwise integration plan (Supplementary Fig. 1). The results suggested that the difficulty with integration of the foreign DNA was specific to the *tpiBA* genes. Since high-level synthesis of the transmembrane proteins might be toxic to the cell, the DNA sequence was modified to lower the expression of these genes. First, the RBS sequences for these genes were redesigned to match the predicted TIRs for the native *tpiBA* genes in *Comamonas* sp. E6 (2841 and 333 a.u. for *tpiB* and *tpiA*, respectively). Additionally, the initial ATG in *tpiB* was replaced with GTG to match that of the native *Comamonas* sp. E6 gene. In this way, the $tphCA_2A_3BA_1$:*tpiBA* genes were integrated into the ADP1 chromosome to generate strain IP130 (Fig. 2B).

Sasoh et al. had previously reported that in a *C. testosteroni* mutant expressing only the $tphA_2A_3BA_1$ catabolic genes from *Comamonas* sp. E6, TPA consumption was favored at pH 6 over pH 7. This was attributed to the partial protonation of carboxylic groups, which would favor passive diffusion of the substrate through the cell membrane (Collier et al., 1997; Vermaas et al., 2019). Therefore, we evaluated the effect of pH on TPA consumption by wild-type ADP1, IP130, and a strain lacking *tpiBA*

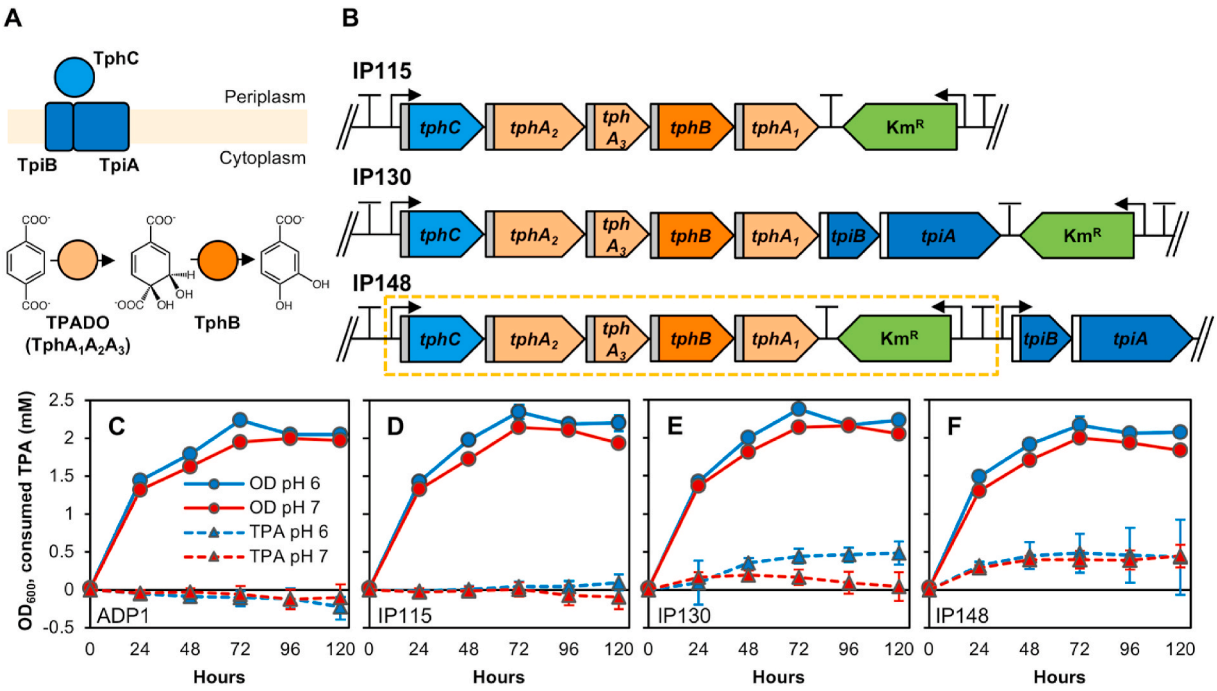

Fig. 2. TPA transport and catabolism, genetic organization, and TPA turnover in *A. baylyi* strains with a single copy of heterologous genes integrated in the chromosome. (A) TPA transport and catabolic proteins from *Comamonas* sp. E6. (B) Schematic representation of the synthetic *tph*:*tpi* operons integrated in the chromosome of ADP1, downstream of *pobA*. Catabolic genes are shown in light orange (*tphA* genes, encoding TPADO) or dark orange (*tphB*, encoding dihydrodiol dehydrogenase). Transport genes are shown in light blue (*tphC*, encoding periplasmic SBP) or dark blue (*tpiBA*, encoding transmembrane proteins). The kanamycin resistance gene is shown in green. Synthetic RBS sequences are shown in gray (high predicted TIR) or white (low predicted TIR). Black arrows indicate transcription initiation and direction. The black "T"s indicate transcription terminators (*rrnB* T1 upstream *tphC* and prophage T4 transcription/translation termination signal flanking the Km^R gene). The EASy amplicon is bound by a dotted line for strain IP148. (C–F) Growth (OD_{600}) and consumed TPA (mM) for (C) wild-type ADP1, (D) IP115, (E) IP130, and (F) IP148, grown in MMP + 5 mM TPA at pH 6 and pH 7. Pyruvate (20 mM) was supplemented every 24 h to support growth and completely consumed in all cases (120 mM in total). Consumed TPA values shown are corrected with respect to non-inoculated flasks to account for the increased TPA concentrations caused by evaporation. Error bars indicate the standard deviation for three replicates.

(IP115, Fig. 2B–E). In contrast to wild type and IP115, IP130 turned over small amounts of TPA (~10%) when pyruvate, which minimizes catabolic repression of aromatic metabolism (Dal et al., 2002; Fischer et al., 2008; Siehler et al., 2007), was provided as a growth substrate. However, all strains presented a Tpa^- phenotype – *i.e.* were unable to grow on TPA as the sole carbon and energy source (Supplementary Fig. 2). As observed by Sasoh et al., the amount of TPA consumed by IP130 was higher at pH 6 than at pH 7 (p-values < 0.05 for a two-tailed t-test between TPA consumed at pH 6 and at pH 7 for 48- through 120-h timepoints). Since no significant consumption of TPA was observed for IP115, these results suggest that, although minimally, TPA uptake might be enhanced when *tpiBA* genes are expressed.

3.2. Gene amplification and adaptive laboratory evolution by EASy

With the aim of developing Tpa^+ strains (*i.e.* capable of growing on TPA as sole carbon and energy source), we next amplified the chromosomal gene dosage of the *tph* genes to initiate ALE. Given the potential toxicity to the cell of synthesizing the transmembrane proteins at a high level, we first reorganized the synthetic operon so that the *tpiBA* genes would not be part of the amplicon (boundaries shown for IP148 in Fig. 2B). As observed for strain IP130, IP148 turned over small amounts of TPA when grown on pyruvate, but remained Tpa^- (Fig. 2F, Supplementary Fig. 2).

IP148 was transformed with the SBF (see Subsection 2.4 for details), which serves as a platform for homologous recombination and precise duplication of chromosomal segments. This duplication enables changes in the number of tandemly arrayed amplicon copies under selective pressure. In this way, transformants with increased gene dosage were first selected on MMP plates with high Km. Selective pressure was then changed to growth on TPA as the sole carbon source, and Tpa^+ colonies arose after ~10 days (in the absence of antibiotics). When these colonies were re-streaked, Tpa^+ colonies appeared more rapidly, after only 2–3 days. Although individual colonies each represent a clonal population, the proclivity of the tandem copies to increase or decrease via recombination suggests that different cells within the colony may differ in amplicon copy number. Frequent recombination also promotes additional genetic change, so that all cells in any Tpa^+ colony may not be genetically identical. Therefore, we hereafter refer to these Tpa^+ mutants as isolates.

Four isolates, designated TPA_1 to TPA_4, were selected to initiate ALE. These were grown in liquid MM with 5 mM TPA, and cultures were serially transferred to enrich for mutations enabling faster growth. Given that lower pH values could advantageously favor diffusion of TPA into the cell, serial transfers for ALE with these isolates were conducted at pH 6 and pH 7 in parallel (8 lineages, designated by .6 or .7 after the isolate name to indicate the pH of the medium used for serial transfer, Fig. 3). The copy number of the amplicon was monitored regularly by qPCR of the Km^R gene to assess whether a reduction in gene dosage resulted from the selection of beneficial mutations that improve cell fitness. After initial serial transfers inoculated by 100-fold dilution every 48 h in 5 mM TPA, the selection pressure for ALE was gradually increased with the aim of improving tolerance, growth, and TPA consumption rates. This was first done by diluting cells 100-fold every 24 h in 5 mM TPA, and then 200-fold every 24 h in 10 mM TPA. The evolution of the gene copy number over time for the eight lineages is shown in Fig. 2.

In parallel with ALE, we also sequenced PCR products amplified from the *tpiBA* genes from IP148 and isolates TPA_1 to TPA_4, to test whether early acquisition of beneficial mutations in the transporter genes could

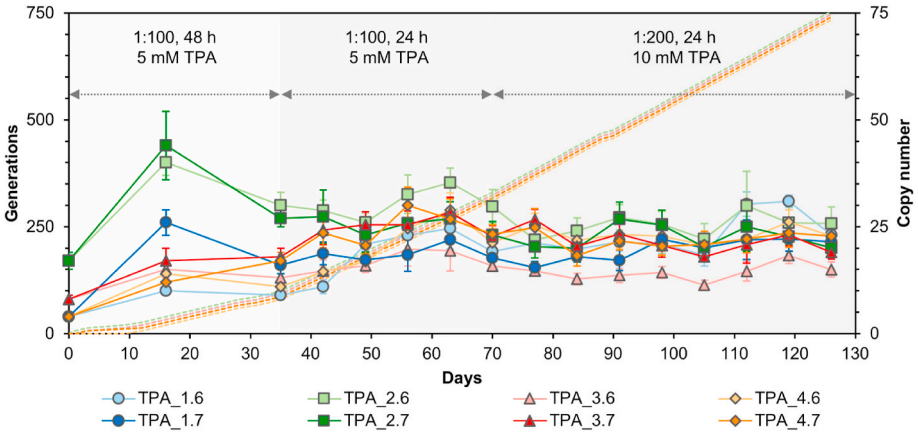

Fig. 3. ALE of IP148-derived amplification mutants on TPA. Symbols indicate changes in amplicon copy number over time (values indicated on the right-side axis). Error bars indicate the standard deviation for four technical replicates. Cumulative generations are shown as dashed lines (values indicated on the left-side axis). Changes in serial transfer conditions (culture dilution, frequency, and TPA concentration) during ALE are indicated.

have enabled growth on TPA. Sequencing revealed that all of them, including parent-strain IP148, carried an unexpected mutation in *tpiA* that would result in a premature stop codon (GAG → UAG, Fig. 4A and Supplementary Fig. 3). This *tpiA1481* allele is predicted to encode a 365-residue peptide [TpiA(W366*)] with an early termination disrupting the 7th transmembrane helix (TMH), in contrast to the 503-residue TpiA protein of 11–12 predicted TMHs. Further inspection of the sequence also revealed that translation could be re-initiated from an in-phase start codon (AUG) only 12 bp downstream of the premature stop codon, with a predicted TIR of 437 a.u. This new coding sequence, referred to as allele *tpiA1482*, would encode a peptide corresponding to the last 133 residues of TpiA [TpiA(Δ1-370)]. Interestingly, no mutations were

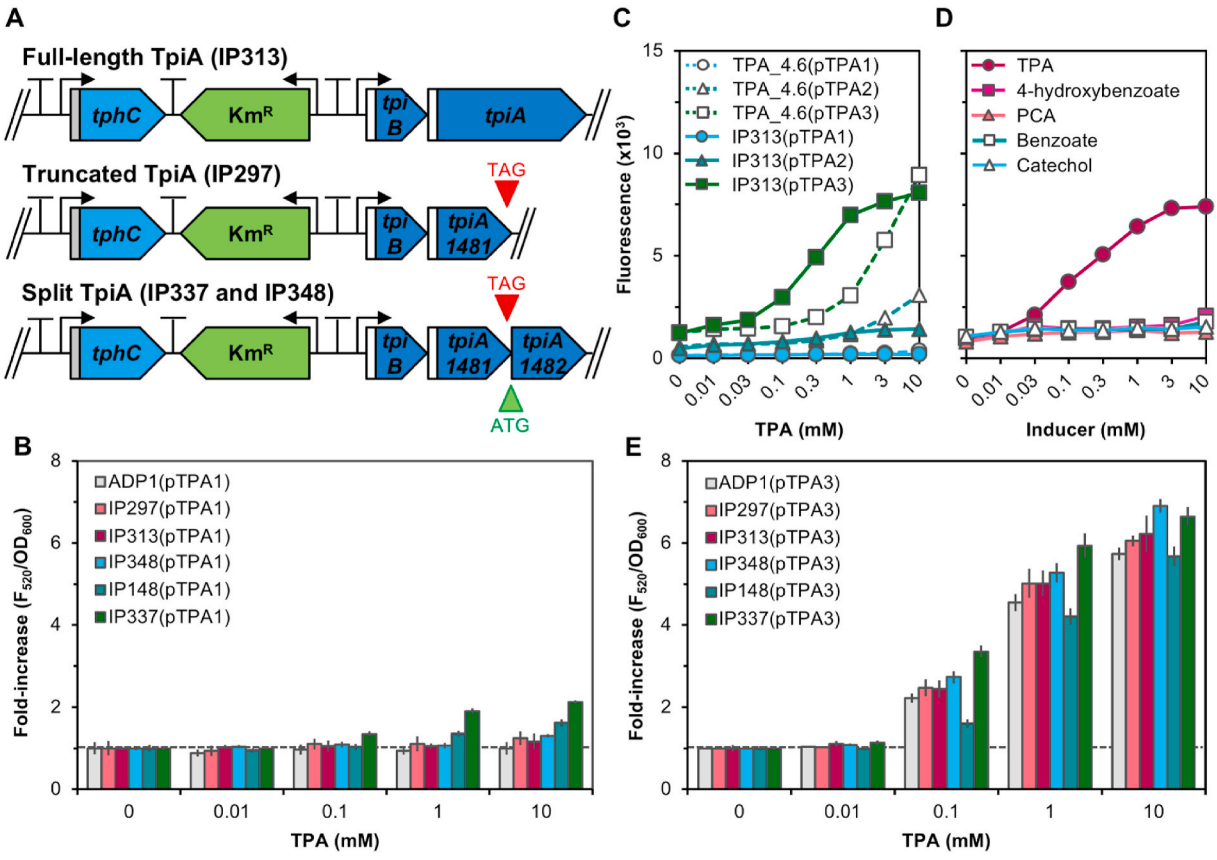

Fig. 4. Biosensor-based evaluation of TPA uptake. (A) Schematic representation of engineered mutants encoding variants of the TPA-TTT, which consists of transmembrane proteins (TpiB and TpiA) and a periplasmic SBP (TphC). (B) Fold-increase of normalized fluorescence at 520 nm (F_{520}/OD_{600}, as measured in a plate-reader; 100 gain, 12-h timepoint) for *A. baylyi* strains carrying pTPA1 and grown in MMP with increasing TPA concentrations. (C) Mean fluorescence, as measured by flow cytometry, for population TPA_4.6 and strain IP313 harboring different generations of TPA sensor plasmids, using increasing concentrations of TPA to induce fluorescence. (D) Specificity of pTPA3 in IP313, using increasing concentrations of TPA, 4-hydroxybenzoate, PCA, benzoate, or catechol to induce fluorescence, and measured by flow cytometry. (E) Fold-increase of normalized fluorescence at 520 nm (F_{520}/OD_{600}, as measured in a plate-reader; 50 gain, 8-h timepoint) for *A. baylyi* strains carrying pTPA3 and grown in MMP with increasing TPA concentrations. Error bars indicate the standard deviation for three biological replicates.

found in the *tpiBA* genes in strain IP130.

3.3. Engineering a fluorescent biosensor to evaluate TPA transport

The results from sequencing raised the question of whether the TPA-TTT was still functional in IP148 and the four Tpa^+ isolates, despite the mutation in *tpiA*. Two possibilities were contemplated. The first was that, due to the internal homology in TpiA, two TpiA(W366*) peptides, each encompassing TMHs 1–6, could form a homo-dimer that enabled TPA transport. Evolutionary studies of TTTs have shown that in homologs of TpiA, the transmembrane helices 1–6 are homologous to TMHs 7–12, suggesting that these proteins originated as a result of gene duplication and fusion (Winnen et al., 2003). The second possibility was that, if re-initiation of translation were to occur downstream of the premature stop codon, the two individually translated peptides, TpiA (W366*) and TpiA(Δ1-370), could associate to restore function. Reconstitution of function of transmembrane proteins expressed from separate gene segments has been reported in the literature (Bibi and Kaback, 1990; Schmidt-Rose and Jentsch, 1997; Zen et al., 1994). Consequently, we sought to evaluate TPA uptake in strains expressing different alleles of *tpiA*.

To evaluate TPA transport, we required a rapid assay that would allow us to screen multiple mutants at the same time. Hence, we embarked on a parallel effort to develop a biosensor for intracellular TPA based on the transcription factor TphR, an IclR-family member which regulates expression of the *tph* operon in *Comamonas* sp. (Kasai et al., 2010). For this purpose, a DNA cassette was constructed with the native *tphR* sequence and its upstream regulatory region that separates its coding sequence from the divergently oriented *tphC*. In place of *tphC*, the gene encoding the sfGFP reporter was inserted in this cassette, such that TphR controls its transcription (Supplementary Fig. 4). For this plasmid-borne biosensor construct, the regulatory region sequence was modified slightly from the native sequence found immediately upstream of the *tphC* coding sequence. The latter contains a derivative of the canonical RBS (AAGGAGA) followed by a short CAAG spacer. In *E. coli* and *P. putida*, we have found that this RBS, coupled with a longer spacer (TATACAT), is effective for engineering biosensors (Jha et al., 2018, 2014). Therefore, we constructed the same combination (AAGGAGA-TATACAT) for the current TPA biosensor.

The first version of this biosensor plasmid (pTPA1) was transformed into ADP1-derived mutants expressing *tphC*, *tpiB*, and different *tpiA* alleles (Table 1, Figs. 1 and 4A). The synthetic operons were designed to resemble the organization in IP148, except that the catabolic genes were not present. The different *tpiA* alleles evaluated included full-length *tpiA* in strain IP313; *tpiA1481* [encoding TpiA(W366*)] in strain IP297; and *tpiA1481* in combination with *tpiA1482* [encoding TpiA(Δ1-370)] in strains IP337 and IP348. Strain IP337 was constructed by deleting the catabolic genes from IP148, whereas IP348 was constructed by *de novo* integration of DNA in a wild-type ADP1 background. The different TpiA variants are referred to as full-length TpiA, truncated TpiA, or split TpiA in Fig. 4A.

When strains carrying pTPA1 were grown in the presence of TPA, a weak fluorescent response (fold-increase in fluorescence relative to uninduced cultures) was observed with increasing TPA concentrations (Fig. 4B). However, the fluorescence signal for most strains was close to the baseline fluorescence obtained in the absence of TPA. The exceptions were the parent-strain IP148 and the strain derived from it by deleting the catabolic genes (IP337). For these strains, there was a 1.5 to 2-fold increase in fluorescence at the highest TPA concentrations (mM range). However, these strains also exhibited higher fluorescence signals relative to the other mutants even in the absence of TPA (Supplementary Fig. 5A), which suggested there could be an unintended mutation in the genome that affected sfGFP expression (Subsection 3.5).

Since the first-generation sensor pTPA1 exhibited a low dynamic range, we optimized it by creating mutated plasmid libraries with changes in the regulatory DNA region upstream of the sfGFP coding sequence. These mutated plasmid libraries were transformed into *A. baylyi* strains expressing different versions of the TPA-TTT in parallel. In previous work we showed that the promoter region (-35 and -10 sites), the RBS, the transcription initiation site (TI), and the distance between the operator and the -35 site constitute the tunable elements that can affect biosensor activity (Jha et al., 2018). Hence, we designed focused libraries targeting different positions in these sites for randomization.

For the second generation of the sensor, we created a library in which both the -35 site (TTAACA) and the -10 site (CATACT) were partially and simultaneously randomized to NTNANA and NANANT, respectively. The variants were evaluated by multiple rounds of FACS with induced and uninduced populations to isolate those with the highest contrast ratios (induced/uninduced fluorescence signal). The best performing variant, hereafter referred to as pTPA2, had three mutations in the -10 site (CATACT → TACAAT) and showed high specificity for TPA (Supplementary Fig. 6).

For the third generation of the sensor, two different libraries were constructed, each one targeting the complete randomization of either the -35 site or the -10 site in pTPA2. Parallel strategies that included three FACS rounds combining the positive sorting from a 0.3 mM TPA-induced population and the negative sorting from the uninduced population converged to a single sequence with improved TPA response over the rest. The selected variant, hereafter pTPA3, had 4 mutations in the -35 site (TTAACA → GTACAC) relative to pTPA2, as well as a deletion between the operator and the -35 site that was unintended in this library but known to affect the dynamic range (Jha et al., 2018, 2014). Conversely, the library where the -10 site was fully randomized did not result in any improvements over pTPA2.

A comparison of the performance of the three generations of sensors pTPA1, pTPA2, and pTPA3 is shown in Fig. 4C. These were simultaneously tested in IP313 and the ALE lineage TPA_4.6 (mixed population evolved for ~600 generations), as the Tpa^+ phenotype of TPA_4.6 ensured that the substrate could be imported into the cell. Attempts to transform the biosensors into other ALE lineages were unsuccessful, most likely due to the loss of competency that occurs in ADP1-derived strains during ALE (Bacher et al., 2006; Renda et al., 2015). The relative improvements observed for pTPA1, pTPA2, and pTPA3 were similar for both strains, with a gradual increase in the maximum fluorescence signal at the expense of a slight increase in the baseline signal. However, the requirement of a higher TPA concentration to elicit a comparable response for TPA_4.6 relative to IP313 most likely reflects its ability to degrade TPA, thereby lowering the effective internal concentration of TPA as an inducer. As with pTPA2, pTPA3 also showed a negligible response towards aromatic compounds similar to TPA, such as benzoate, 4-hydroxybenzoate, PCA, and catechol, confirming the high specificity of the sensor for TPA (Fig. 4D).

We then re-evaluated *A. baylyi* strains encoding the different variants of the TPA-TTT using the improved pTPA3 sensor (Fig. 4E). In contrast to our expectation, the fluorescent response in all strains were comparable. In fact, wild-type ADP1, which does not encode a TPA-TTT, also responded to increasing TPA concentrations. Nevertheless, the reduced response of IP148 with respect to IP337 and IP348 (all encoding the split TpiA variant) suggested that the biosensor was sufficiently sensitive to detect the turnover of small amount of TPA when the *tph* catabolic genes were expressed from a single copy in IP148. It should also be noted that, in the absence of TPA, IP148 and IP337 still exhibited higher fluorescence signals relative to other strains (Supplementary Fig. 6B), as observed with pTPA1. This observation supported the hypothesis that the increased fluorescence signal in these two strains was independent of TPA uptake or the sensor plasmid, and instead was likely due to a mutation in the genome that affected expression of the sfGFP gene.

In all, no significant differences were found between ADP1-derived strains expressing different alleles of *tpiA* (*i.e.* IP297, IP313, and IP348). Furthermore, their fluorescent response was barely above that of wild type. We also note that no differences in growth rates were

observed for any of the strains at the TPA concentrations tested. These results suggest that the heterologous TPA-TTT would have a minimal role in TPA uptake in *A. baylyi*, and that the evolved TPA$^+$ isolates could instead be importing this substrate through an unidentified, native transporter.

3.4. Phenotypic characterization of evolved A. baylyi isolates

After ~100 transfers of ALE (~750 generations), the copy number of the amplicon stabilized at 15–25 copies without substantial changes in growth rates (Fig. 3, Supplementary Fig. 7). Therefore, single colonies were isolated from each lineage for phenotypic characterization and WGS. The copy-number ratio of *tphA*$_2$ over the Km^R gene for the selected isolates was confirmed to be of ~1, suggesting that qPCR of the latter accurately estimates the copy number of the entire amplicon defined by the SBF (Supplementary Fig. 8). Shake-flask cultures of early ALE populations (~30 generations) and post-evolution isolates showed that growth rates and TPA consumption rates were enhanced (Fig. 5), except for populations TPA_2.6 and TPA_2.7 and their respective evolved isolates IP247 and IP250 (Fig. 5C, D). However, it is notable that the amplicon copy number in these populations had decreased from ~40 to ~20 copies during ALE (Fig. 3, Supplementary Fig. 7). An important decrease in the lag-phase was also observed, especially in the case of IP254 with respect to early population TPA_3.7 (Fig. 5F). Moreover, tolerance to increasing TPA concentrations was enhanced in several evolved strains (Supplementary Fig. 9). No important phenotypic differences were observed between isolates derived from the parallel evolution at pH 6 compared to that at pH 7, although growth and TPA utilization appeared to be slightly faster at pH 6 than at pH 7.

We also compared the evolved *A. baylyi* isolates to the native TPA-utilizing bacteria *Comamonas* sp. E6 and *R. jostii* RHA1, both grown at the standard pH 7 (Fig. 6 and Supplementary Table 6). Growth and TPA consumption rates of the evolved Tpa$^+$ isolates were slightly lower than those of *Comamonas* sp. E6 (an average of 0.40 h^{-1} and 0.20 g/L/h, respectively, in the evolved *A. baylyi* isolates, compared to 0.50 h^{-1} and 0.26 g/L/h in *Comamonas* sp. E6), which was the source of the catabolic and TTT genes expressed in the engineered *A. baylyi* strains. In contrast, the evolved isolates out-performed *R. jostii* RHA1, which had a 12-h lag phase, a 0.26 h^{-1} growth rate and a 0.13 g/L/h TPA consumption rate. Specific consumption rate values for the evolved isolates (~1 g TPA/g cells/h in average) were also between those of *Comamonas* sp. E6 (1.55 g/g/h) and *R. jostii* RHA1 (0.46 g/g/h) (Supplementary materials and methods and Supplementary Table 6).

3.5. Whole-genome sequence analysis of evolved A. baylyi isolates

To identify mutations that might be responsible for their improved growth on TPA, WGS was performed for each of the evolved isolates selected from the eight lineages. A complete list of the mutations found in the IP148 parent strain, relative to the published sequence for wild-type ADP1, and in each evolved isolate is provided in Supplementary Excel-1. Results are summarized in Supplementary Table 7. The increased coverage for certain regions of the chromosome revealed unexpected duplications and amplifications different than the one targeted by EASy. For example, a region of ~10 kb (corresponding approximately to positions 1,849,000–1,858,000 in NCBI reference sequence NC_005966), comprising several duplicate genes coding for hypothetical proteins, is amplified in the parent strain IP148 and maintained in all evolved derivatives. IP251 and IP254 (both derived from TPA_3) show a spontaneous amplification of a ~56 kb fragment (corresponding approximately to positions 1,670,000–1,727,000 in the reference sequence) directly upstream of the insertion site of the synthetic *tph*:*tpi* operon, that includes the *dca*, *pca*, *qui*, and *pob* gene clusters. These gene clusters are respectively involved in the metabolism of saturated C_6–C_{10} dicarboxylic acids, PCA, quinic acid, and 4-hybroxybenozoic acid, all of which are metabolized via the β-ketoadipate pathway (Fischer et al., 2008; Young et al., 2005).

As observed in the phenotypic characterization of the evolved isolates, there were no clear trends in the mutations found for the lineages evolved at pH 6 or at pH 7, except for an in-phase tandem repeat in the gene coding for an EpsG family protein (ACIAD_RS00385) that was present in 3 out of the 4 isolates evolved at pH 6 and absent in all those evolved at pH 7 (Supplementary Table 7). The mutation in *tpiA*, initially identified in the parent-strain IP148 and the amplified derivatives that

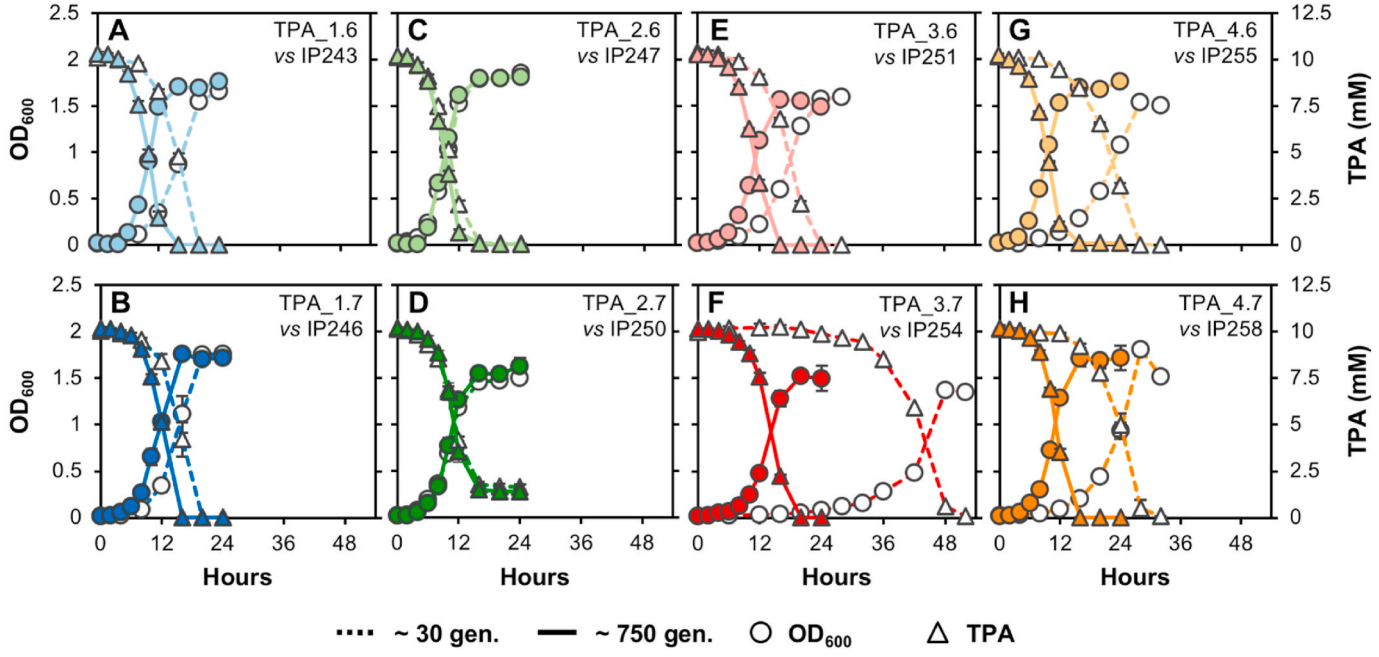

Fig. 5. Shake-flask cultures with TPA as a sole carbon and energy source. Growth (OD_{600}) and TPA concentration (mM) over time are plotted for cultures of EASy lineages after ~30 generations and isolates after ~750 generations. Cultures from top (A, C, E, G) and bottom (B, D, F, H) rows were respectively grown at pH 6 and pH 7. Error bars indicate the standard deviation from three biological replicates.

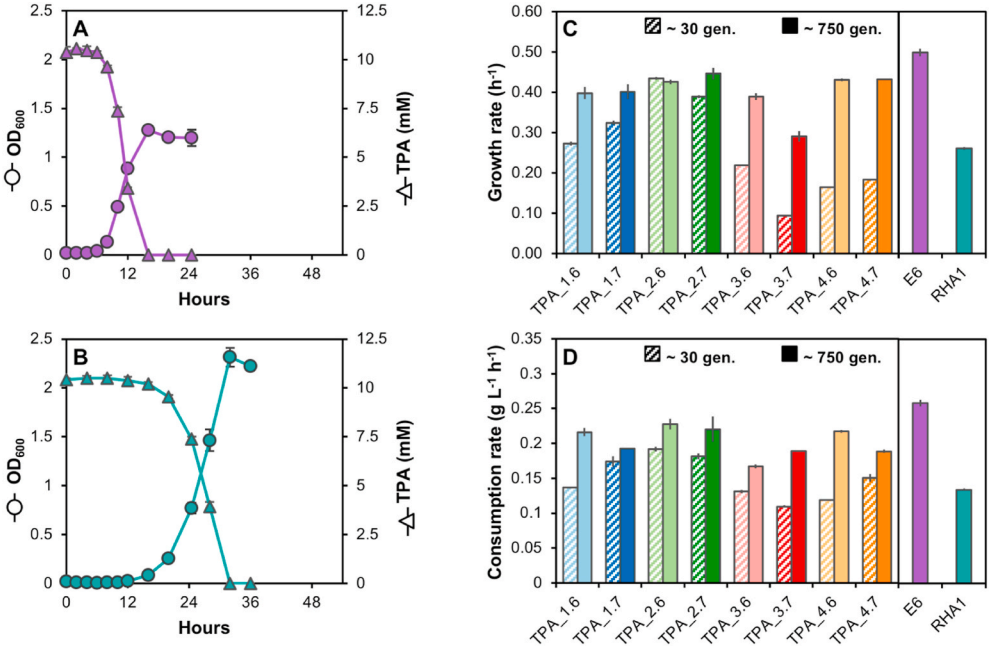

Fig. 6. Comparison of *A. baylyi* EASy lineages after ~30 generations and isolates after ~750 generations to native TPA-utilizing bacteria. (A–B) Growth (OD_{600}) and TPA concentration (mM) over time for (A) *Comamonas* sp. E6 and (B) *R. jostii* RHA1 cultures grown at pH 7. (C) Growth rates (h^{-1}), calculated from $ln(OD_{600})$ as a function of time. (D) TPA consumption rates (g/L/h) calculated from TPA concentration as a function of time in log growth phase. Error bars indicate the standard deviation from three biological replicates.

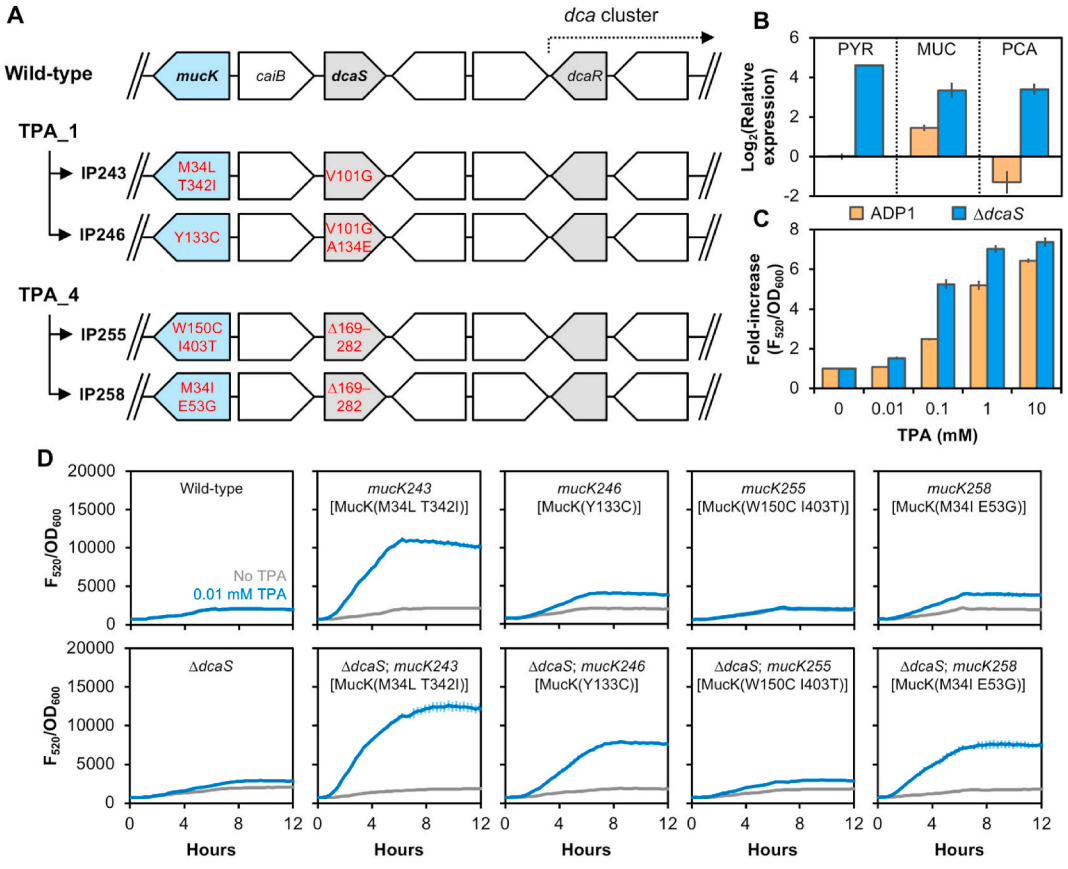

Fig. 7. Evaluation of mutations in *mucK* and *dcaS*. (A) Schematic representation of *mucK* and *dcaS* mutations found in evolved isolates, showing their genetic organization in the chromosome. Predicted amino acid changes are shown in red. (B) Relative *mucK* expression levels ($2^{-\Delta\Delta Ct}$) for wild-type ADP1 and Δ*dcaS* mutant IP461. Results are shown for three biological replicates, each measured with three technical replicates, and normalized to wild-type ADP1 grown on pyruvate. Error bars indicate the standard deviation. PYR: pyruvate; MUC: muconate; PCA: protocatechuate. (C) Fold-increase of normalized fluorescence at 520 nm (F_{520}/OD_{600}) for wild-type ADP1 and Δ*dcaS* mutant IP461, both transformed with pTPA3, after 8 h of growth in MMP with increasing TPA concentrations. Error bars indicate the standard deviation for biological triplicates. (D) Normalized fluorescence (F_{520}/OD_{600}) over time for *mucK* mutant strains in wild-type or Δ*dcaS* backgrounds, transformed with pTPA3, and grown in the absence (gray lines) or presence of 0.01 mM TPA (blue lines). MucK variants encoded by the different alleles are indicated in brackets. Average and standard deviation for biological triplicates are shown.

were used to initiate ALE (TPA_1 to TPA_4), was maintained in all evolved isolates. This fact suggests that this mutation, potentially encoding a truncated or split TpiA, was not disadvantageous for growth on TPA. Unexpectedly, no mutations were found in the *tph* genes, except for a single nucleotide change in the synthetic RBS sequence preceding $tphA_3$ in IP251 and IP254, both derived from TPA_3. Nevertheless, it should be noted that the short reads provided by the Illumina sequencing method do not allow the detection of mutations that might be present in only one of the multiple copies of the amplicon and that could be beneficial for growth on TPA.

Another mutation identified in the parent-strain IP148 encoded a variant of the RNA polymerase sigma-70 factor, RpoD(A87E). This mutation was maintained in all evolved isolates except IP246 (Supplementary Table 7). A different mutation in *rpoD* results in a growth deficit in ADP1 (Suárez et al., 2017). However, a growth competition experiment showed that RpoD(A87E) was only minimally detrimental to growth (Supplementary materials and methods and Supplementary Fig. 10). Residue A87 is located in region 1.1 of RpoD, which is involved in promoter binding (Bowers et al., 2000). Therefore, this mutation could potentially affect transcription efficiency in the cell. Indeed, when the mutated *rpoD* was replaced by the wild-type allele in IP148 derivatives, the high baseline fluorescence observed when transformed with the biosensor plasmid pTPA3 was reduced (Subsection 3.3 and Supplementary Fig. 10). As RpoD is the primary or "housekeeping" sigma factor in many bacteria, it is possible that this mutation alters the gene expression profile in ADP1 (Choe et al., 2019). Additional experiments to confirm this possibility are needed.

Further analysis of WGS data revealed that 4 out of the 8 isolates (derived from TPA_1 and TPA_4) had mutations in *mucK* (ACIAD_RS07750) in combination with mutations in *dcaS* (ACIAD_RS07760), which are two genes in close proximity in the chromosome (Fig. 7A). Moreover, the spontaneous amplification of the *dca-pca-qui-pob* supraoperonic cluster in IP251 and IP254 (derived from TPA_3) included the *mucK* and *dcaS* genes. These two isolates also had a mutation in the *mucK-caiB* intergenic region. The prevalence of mutations in these loci suggested that MucK and DcaS may have a relevant role in the Tpa^+ phenotype.

A DcaS homolog from *Brucella abortus*, also an IclR-type regulator, has been identified as a repressor of adipic acid metabolism therein, and its crystal structure has been solved (Herrou et al., 2018). Using this structure as template (PDB 5WHM, 62% sequence identity), three-dimensional structure models of DcaS were built to examine the location of the amino acid replacements encoded by the different evolved isolates (Supplementary Fig. 11). In the case of IP243 and IP246, these replacements are located in the predicted α-helical linker involved in dimerization (V101G) and the ligand-binding pocket (A134E). In IP255 and IP258, the deletion of bases 499 and 500 in the *dcaS* coding sequence causes a shift in the open reading frame. The resulting DcaS variant would lack residues 169–282, which form part of the ligand-binding domain. Based on this analysis, these amino acid changes are predicted to disrupt DcaS function.

While there were conserved *dcaS* mutations in evolved isolates derived from the same initial Tpa^+ mutant, *mucK* mutations were different in all cases, suggesting that mutations in *dcaS* appeared before those in *mucK* (Fig. 7A). MucK is a MFS muconate transporter in ADP1 (Williams and Shaw, 1997), and it belongs to the same superfamily as the TPA transporters from *Rhodococcus* species and *P. xenovorans*. Therefore, we hypothesized that MucK and its variants are capable of transporting TPA in *A. baylyi*. Furthermore, the potential loss of DcaS function in the evolved isolates, seemingly preceding the mutation of *mucK*, suggested that DcaS acts as a repressor of *mucK* transcription.

A similar combination of mutations in genes encoding a transcriptional regulator and a MFS transporter is found in evolved isolates IP247 and IP250 (both derived from TPA_2). These isolates share a ~100 bp deletion in a gene encoding a FadR-family transcriptional regulator (ACIAD_RS00620 locus). In contrast, they have two different mutations in a neighboring gene predicted to encode a glucarate/galactarate MFS transporter (*gudP*, ACIAD_RS00595 locus). These mutations lead to amino acid replacements R289C in IP247 and R447L in IP250 (Supplementary Table 7). However, we decided to focus on *mucK* and *dcaS* for further evaluation, as they had apparently co-evolved in separate lineages.

3.6. Evaluation of MucK as a TPA transporter and its regulation by DcaS

To test our hypothesis that MucK was importing TPA, we first attempted to knock out its coding gene in the eight evolved isolates. However, due to a presumed loss of natural competency, we were only able to knock out *mucK* in IP243 and IP255, 2 out of the 4 isolates that had mutations in this gene. Consistent with our hypothesis, these mutants lost the ability to grow on either muconate (Muc^- phenotype) or TPA (Supplementary Fig. 12).

We then tested whether the deletion of *dcaS* and/or replacement of wild-type *mucK* with the four alleles selected during ALE enabled growth of the IP148 parent strain on TPA (Table 2). The resulting IP148-derived mutants were inoculated in MM with 10 mM TPA as a sole carbon and energy source. After an incubation of 1–2 weeks, 8 out of 9 mutant cultures started growing and reached saturation in 24–48 h, indicating that each of these genetic modifications was sufficient to enable growth on TPA. The exception was strain IP402, carrying the allele encoding MucK(W150C I403T), which unexpectedly also presented a Muc^- phenotype. However, when this allele was expressed in a Δ*dcaS* background (strain IP417), Muc^+ and Tpa^+ phenotypes were observed, indicating that MucK(W150C I403T) was still functional. As expected, control mutants IP367 and IP387 with *mucK* knocked out were Tpa^- and Muc^-, even if *dcaS* was deleted in the latter. Consistent with previous observations, no growth on TPA was observed for parent-strain IP148 after 2 weeks of incubation.

Given the natural propensity of bacteria to undergo spontaneous gene duplication and amplification to increase gene expression under selective pressure (Andersson and Hughes, 2009; Elliott et al., 2013), we tested whether these IP148-derived Tpa^+ mutants still retained a single copy of the synthetic *tph* operon or if it had been duplicated. For this purpose, we collected the Tpa^+ cells from the TPA cultures indicated in Table 2 to evaluate the copy number by qPCR. Unlike the case of the Tpa^+ strains obtained by transformation with an SBF to delimit the amplicon, it was possible that in these new mutants an amplified chromosomal region may not include the Km^R gene. Therefore, we used primers and a probe specific for $tphA_2$. We found that, indeed, all Tpa^+ mutants had 6–14 copies of $tphA_2$ (Supplementary Fig. 13). This result indicates that the deletion of *dcaS* and/or expression of different *mucK* alleles is sufficient to enable growth on TPA, but that multiple copies of the *tph* catabolic genes are needed to sustain growth of *A. baylyi* on TPA as sole carbon and energy source.

Table 2
Growth on muconate (Muc phenotype) and TPA (Tpa phenotype) of IP148-derived *dcaS* and *mucK* mutants.

Strain	Mutations	MucK variant	Phenotype	
			Muc	Tpa
IP148	None	Native	+	–
IP367	Δ*mucK*::Sm^R:*sacB*	None	–	–
IP378	Δ*dcaS*	Native	+	+
IP387	Δ*dcaS* Δ*mucK*::Sm^R:*sacB*	None	–	–
IP398	Δ*mucK*::*mucK258*	M34I E53G	+	+
IP400	Δ*mucK*::*mucK243*	M34L T342I	+	+
IP402	Δ*mucK*::*mucK255*	W150C I403T	–	–
IP411	Δ*mucK*::*mucK246*	Y133C	+	+
IP413	Δ*dcaS* Δ*mucK*::*mucK258*	M34I E53G	+	+
IP415	Δ*dcaS* Δ*mucK*::*mucK243*	M34L T342I	+	+
IP417	Δ*dcaS* Δ*mucK*::*mucK255*	W150C I403T	+	+
IP419	Δ*dcaS* Δ*mucK*::*mucK246*	Y133C	+	+

The apparent sequential emergence of *dcaS* and *mucK* mutations in the EASy lineages derived from TPA_1 and TPA_4, and the observation that deletion of *dcaS* alone enabled a Tpa^+ phenotype in IP148-derived mutants, strongly suggested that DcaS acts as a repressor of the transcription of *mucK*. To test this hypothesis, we used RT-qPCR in wild-type ADP1 and a Δ*dcaS* mutant (IP461) grown on 20 mM pyruvate, 10 mM muconate, or 10 mM PCA. In wild-type ADP1, transcription of *mucK* is induced in the presence of muconate when compared to an unrelated carbon source, *i.e.* pyruvate (Fig. 7B). Conversely, transcription of *mucK* is constitutive for all conditions in the Δ*dcaS* strain IP461, confirming our hypothesis that DcaS is a transcriptional repressor of *mucK*. Additionally, a slight repression of *mucK* transcription in the presence of PCA was observed in wild-type ADP1, suggesting that the generation of this intermediate during TPA catabolism could impede further uptake of TPA by MucK. This effect might explain why mutations that inactivate DcaS were selected early on during ALE.

Next, we evaluated how deletion of *dcaS* affected TPA uptake using our biosensor. For this assessment, we transformed the third-generation TPA biosensor pTPA3 into IP461 and compared the fluorescent response to increasing TPA concentrations to that of wild-type ADP1 (Fig. 7C). Indeed, the Δ*dcaS* strain IP461 exhibited higher fluorescence at lower TPA concentrations, and a significant fluorescent response above baseline (no TPA) was detected for this strain in as low as 0.01 mM TPA (p-value <0.001 for a two-tailed t-test). The results obtained for IP461 are in clear contrast to those presented in Fig. 4 for the TPA-TTT mutants, further supporting the hypothesis that the heterologous transporter has a minimal impact in TPA uptake in ADP1.

Finally, we sought to assess how mutations in *mucK* affected uptake of TPA in the presence or absence of DcaS. Hence, we replaced the native *mucK* gene in either wild-type ADP1 or IP461 backgrounds, transformed all strains with pTPA3, and evaluated fluorescence in the presence or absence of TPA. In order to detect differences in uptake efficiency between the different MucK variants, we induced expression of the sfGFP gene with 0.01 mM TPA, the lowest concentration tested at which wild-type ADP1 did not exhibit a fluorescent response but IP461 did (Fig. 7C). As shown in Fig. 7D, the expression of all mutated *mucK* alleles, except that encoding MucK(W150C I403T), resulted in an increased extent of fluorescence in the presence of TPA. These results demonstrate that at least 3 of the 4 MucK variants that arose during ALE are more efficient in TPA uptake than native MucK. Furthermore, the increased fluorescent response was synergistic with the deletion of *dcaS*, which is consistent with our finding that deletion of this transcription factor increases expression of *mucK*.

4. Discussion

In this work, our goal was to engineer *A. baylyi* ADP1 to grow on TPA as a sole carbon and energy source using EASy with the *tph* catabolic genes from *Comamonas* sp. E6, a native TPA-utilizing bacterium. To that end, we successfully evolved *A. baylyi* strains for improved growth and consumption rates on this substrate. However, in contrast to our previous work (Tumen-Velasquez et al., 2018), ALE through serial transfer did not lead to the isolation of Tpa^+ strains with less than ~15 copies of the *tph* catabolic operon. While WGS of evolved isolates identified beneficial mutations that enabled growth of ADP1 mutants on TPA (*i.e.* in *dcaS* and *mucK*), none of these were found to lie within the exogenous catabolic or transporter genes. Furthermore, the reintroduction of these beneficial mutations in the parent strain IP148 still led to the spontaneous amplification of the *tph* genes upon selection for growth on TPA (Table 2 andSupplementary Fig. 13). These results demonstrate that ADP1 requires multiple copies of these genes to support growth on TPA as sole carbon and energy source, and highlight the benefit of gene amplification as a natural mechanism employed by microorganisms to rapidly increase gene expression in response to an abrupt selective pressure (Andersson and Hughes, 2009; Elliott et al., 2013; Seaton et al., 2012; Tomanek et al., 2020).

Interestingly, the TPA catabolic gene clusters in TPA-utilizing bacteria *Comamonas* sp. E6, *R. jostii* RHA1, and *Rhodococcus* sp. DK17 are duplicated in the genomes of these organisms (Choi et al., 2005; Hara et al., 2007; Sasoh et al., 2006). Additionally, the presence of transposable elements and DNA modifying genes (integrases, recombinases, and reverse transcriptases) in the immediate vicinity of the TPA operons in these three bacteria and in *D. tsurhuratensis* (*de visu* inspection of publicly available sequences) suggest that these may have been acquired through horizontal gene transfer (McLeod et al., 2006). Considering the xenobiotic nature of TPA, it is likely that TPA catabolism has appeared recently, and that it has not yet fully evolved to be as efficient as the catabolism of other aromatic compounds that are ubiquitous in nature, such as those derived from lignin. In this sense EASy, by combining increased gene dosage and ALE, mimics how new catabolic pathways can evolve in nature: acquisition of exogenous genes through horizontal gene transfer, duplication of the acquired genes to overcome limitations in expression, and/or selection of mutations in the acquired or native genes that enable new functions.

In particular, here we have identified variants of the ADP1 muconate MFS transporter MucK that are more efficient at importing TPA. It should be stressed that this discovery would not have been possible without amplification of the *tph* catabolic genes by EASy, which enabled the growth on TPA that was needed to initiate ALE. Of note, WGS data hint that GudP, another MFS transporter predicted to transport glutarate/galactarate, could have also evolved to transport TPA in the engineered strains. The fact that both transporters are involved in the uptake of dicarboxylic acid suggests that they have a latent activity towards TPA that was improved through ALE (Guzmán et al., 2019). As there are no predicted TTTs in ADP1, it is possible that the transmembrane proteins TpiBA from *Comamonas* sp. E6 are not properly folded or sufficiently active in the heterologous host, and that ADP1 would instead favor MFS transporters to import TPA. However, alignments for MucK and GudP against known TPA MFS transporters (*i.e.* TpaK) from *Rhodococcus* sp. or *P. xenovorans* show sequence identities below 26% (Supplementary Fig. 14). Therefore, the prediction of this latent function by sequence analysis alone would have been improbable. The improved MucK variants identified here expand the known toolset of transporters that can be expressed in heterologous hosts to enable TPA uptake.

In this work, we have also discovered that the transcription factor DcaS represses expression of MucK and that PCA, a metabolite generated during TPA catabolism, could also inhibit the expression of this transporter. Cross-regulation between the catechol (*cat* gene cluster) and PCA (*pca* gene cluster) branches of the β-ketoadipate pathway in ADP1, which will favor the former, are well documented in the literature (Bleichrodt et al., 2010; Brzostowicz et al., 2003; Siehler et al., 2007). However, their interaction with the *dca* gene cluster, involved in the catabolism of saturated C_6–C_{10} dicarboxylic acids (Parke et al., 2001), has not been extensively studied. It should be noted that the *dca* gene cluster encodes another IclR-type regulator, DcaR (Fischer et al., 2008), that could add another layer of regulation that has not been elucidated in the present study (Fig. 7A). Further analysis of the cross-talk between the different branches of the β-ketoadipate pathway would be of interest when engineering the metabolism of ADP1 towards substrates that are funneled through this pathway such as TPA, as cross-regulation could affect productivity and yields in bioprocesses aimed at the conversion of these substrates into value-added bioproducts (Beckham et al., 2016; Johnson et al., 2019).

Finally, we also report the development of a highly sensitive and specific TPA biosensor. The use of biosensors in combination with FACS is becoming an increasingly more frequent approach in metabolic engineering efforts, as it allows the *in vivo*, ultra-high throughput screening of vast mutant libraries and the isolation of top producing cells for the metabolite of interest (Bentley et al., 2020; Rogers and Church, 2016; Zhang et al., 2015). These transcription factor-based sensors, which can respond to intracellular concentrations of a molecule of interest, are also a powerful tool for the discovery of transporters (Genee et al., 2016).

While here we have used the TPA biosensor to study TPA uptake in ADP1, we further propose its potential use for the evaluation of TPA biosynthetic pathways (Luo and Lee, 2017) or the screening of enzymes that generate TPA as a degradation product, such as PET-hydrolyzing enzymes, which we will report in future studies. To date, evaluation of PETase and MHETase activity on their actual substrates, rather than a surrogate, is limited to low-throughput and time-consuming analytical methods (Austin et al., 2018; Han et al., 2017; Joo et al., 2018; Palm et al., 2019). We posit that the biosensor developed in this work, in combination with the ADP1 mutants with improved TPA uptake, could enable fast and simple high-throughput screening of putative PETase and MHETase genes, as well as of large variant libraries aimed at improving the activity of these enzymes. Overall, this work emphasizes the potential of ADP1 as a useful host for metabolic and protein engineering, and provides valuable tools for future efforts in the biological upcycling of PET.

Declaration of competing interest

The authors declare competing financial interest. IP, RKJ, EN, TD, CWJ, and GTB have submitted patent applications that include biosensors and engineered strains described in this work.

Acknowledgments

This work was authored in part by Alliance for Sustainable Energy, LLC, the manager and operator of the National Renewable Energy Laboratory for the U.S. Department of Energy (DOE) under Contract No. DE-AC36-08GO28308. This work has also been authored in part by employees of Triad National Security, LLC, operator of the Los Alamos National Laboratory under Contract No.89233218CNA000001 with the U.S. Department of Energy. Funding was provided by the U.S. Department of Energy Office of Energy Efficiency and Renewable Energy Bioenergy Technologies Office (EERE-BETO) for the Agile BioFoundry to T. D. (Contract NL0032182) and G.T.B. Funding was also provided by NSF grant MCB1615365 to E.L.N. This research used resources provided by the Los Alamos National Laboratory Institutional Computing Program (under w19_proteng to R.K.J), which is supported by the U.S. Department of Energy National Nuclear Security Administration under Contract No. 89233218CNA000001. We thank Jay Fitzgerald at DOE and members of the Agile BioFoundry for helpful discussions. We thank Chantel Duscent-Maitland for technical assistance, and Stacy Bedore, Alyssa Baugh, Melissa Tumen-Velasquez, Nicholas Rorrer, and Joshua Vermaas for helpful discussions.

Appendix A. Supplementary data

Supplementary data to this article can be found online at https://doi.org/10.1016/j.ymben.2020.09.009.

References

Andersson, D.I., Hughes, D., 2009. Gene amplification and adaptive evolution in bacteria. Annu. Rev. Genet. 43, 167–195. https://doi.org/10.1146/annurev-genet-102108-134805.

Austin, H.P., Allen, M.D., Donohoe, B.S., Rorrer, N.A., Kearns, F.L., Silveira, R.L., Pollard, B.C., Dominick, G., Duman, R., Omari, K. El, Mykhaylyk, V., Wagner, A., Michener, W.E., Amore, A., Skaf, M.S., Crowley, M.F., Thorne, A.W., Johnson, C.W., Lee Woodcock, H., McGeehan, J.E., Beckham, G.T., 2018. Characterization and engineering of a plastic-degrading aromatic polyesterase. Proc. Natl. Acad. Sci. U.S. A. 115, E4350–E4357. https://doi.org/10.1073/pnas.1718804115.

Bacher, J.M., Metzgar, D., De Crécy-Lagard, V., 2006. Rapid evolution of diminished transformability in *Acinetobacter baylyi*. J. Bacteriol. 188, 8534–8542. https://doi.org/10.1128/JB.00846-06.

Beckham, G.T., Johnson, C.W., Karp, E.M., Salvachúa, D., Vardon, D.R., 2016. Opportunities and challenges in biological lignin valorization. Curr. Opin. Biotechnol. 42, 40–53. https://doi.org/10.1016/j.copbio.2016.02.030.

Bentley, G.J., Narayanan, N., Jha, R.K., Salvachúa, D., Elmore, J.R., Peabody, G.L., Black, B.A., Ramirez, K., De Capite, A., Michener, W.E., Werner, A.Z., Klingeman, D. M., Schindel, H.S., Nelson, R., Foust, L., Guss, A.M., Dale, T., Johnson, C.W., Beckham, G.T., 2020. Engineering glucose metabolism for enhanced muconic acid production in *Pseudomonas putida* KT2440. Metab. Eng. 59, 64–75. https://doi.org/10.1016/j.ymben.2020.01.001.

Bibi, E., Kaback, H.R., 1990. In vivo expression of the *lacY* gene in two segments leads to functional lac permease. Proc. Natl. Acad. Sci. 87, 4325–4329. https://doi.org/10.1073/pnas.87.11.4325.

Biggs, B.W., Bedore, S.R., Arvay, E., Huang, S., Subramanian, H., McIntyre, E.A., Duscent-Maitland, C.V., Neidle, E.L., Tyo, K.E.J., 2020. Development of a genetic toolset for the highly engineerable and metabolically versatile *Acinetobacter baylyi* ADP1. Nucleic Acids Res. 1–14. https://doi.org/10.1093/nar/gkaa167.

Bleichrodt, F.S., Fischer, R., Gerischer, U.C., 2010. The β-ketoadipate pathway of *Acinetobacter baylyi* undergoes carbon catabolite repression, cross-regulation and vertical regulation, and is affected by Crc. Microbiology 156, 1313–1322. https://doi.org/10.1099/mic.0.037424-0.

Bowers, C.W., McCracken, A., Dombroski, A.J., 2000. Effects of amino acid substitutions at conserved and acidic residues within region 1.1 of *Escherichia coli* σ^{70}. J. Bacteriol. 182, 221–224. https://doi.org/10.1128/JB.182.1.221-224.2000.

Bryksin, A.V., Matsumura, I., 2010. Rational design of a plasmid origin that replicates efficiently in both Gram-positive and Gram-negative bacteria. PloS One 5, e13244. https://doi.org/10.1371/journal.pone.0013244.

Brzostowicz, P.C., Reams, A.B., Clark, T.J., Neidle, E.L., 2003. Transcriptional cross-regulation of the catechol and protocatechuate branches of the beta-ketoadipate pathway contributes to carbon source-dependent expression of the *Acinetobacter* sp. strain ADP1 *pobA* gene. Appl. Environ. Microbiol. 69, 1598–1606. https://doi.org/10.1128/AEM.69.3.1598-1606.2003.

Chain, P.S.G., Denef, V.J., Konstantinidis, K.T., Vergez, L.M., Agullo, L., Reyes, V.L., Hauser, L., Cordova, M., Gomez, L., Gonzalez, M., Land, M., Lao, V., Larimer, F., LiPuma, J.J., Mahenthiralingam, E., Malfatti, S.A., Marx, C.J., Parnell, J.J., Ramette, A., Richardson, P., Seeger, M., Smith, D., Spilker, T., Sul, W.J., Tsoi, T.V., Ulrich, L.E., Zhulin, I.B., Tiedje, J.M., 2006. *Burkholderia xenovorans* LB400 harbors a multi-replicon, 9.73-Mbp genome shaped for versatility. Proc. Natl. Acad. Sci. 103, 15280–15287. https://doi.org/10.1073/pnas.0606924103.

Choe, D., Lee, J.H., Yoo, M., Hwang, S., Sung, B.H., Cho, S., Palsson, B., Kim, S.C., Cho, B. K., 2019. Adaptive laboratory evolution of a genome-reduced *Escherichia coli*. Nat. Commun. 10 https://doi.org/10.1038/s41467-019-08888-6.

Choi, K.Y., Kim, D., Sul, W.J., Chae, J.-C., Zylstra, G.J., Kim, Y.M., Kim, E., 2005. Molecular and biochemical analysis of phthalate and terephthalate degradation by *Rhodococcus* sp. strain DK17. FEMS Microbiol. Lett. 252, 207–213. https://doi.org/10.1016/j.femsle.2005.08.045.

Collier, L.S., Nichols, N.N., Neidle, E.L., 1997. *benK* encodes a hydrophobic permease-like protein involved in benzoate degradation by *Acinetobacter* sp. strain ADP1. J. Bacteriol. 179, 5943–5946. https://doi.org/10.1128/jb.179.18.5943-5946.1997.

Dal, S., Steiner, I., Gerischer, U., 2002. Multiple operons connected with catabolism of aromatic compounds in *Acinetobacter* sp. strain ADP1 are under carbon catabolite repression. J. Mol. Microbiol. Biotechnol. 4, 389—404.

de Berardinis, V., Vallenet, D., Castelli, V., Besnard, M., Pinet, A., Cruaud, C., Samair, S., Lechaplais, C., Gyapay, G., Richez, C., Durot, M., Kreimeyer, A., Le Fèvre, F., Schächter, V., Pezo, V., Döring, V., Scarpelli, C., Médigue, C., Cohen, G.N., Marlière, P., Salanoubat, M., Weissenbach, J., 2008. A complete collection of single-gene deletion mutants of *Acinetobacter baylyi* ADP1. Mol. Syst. Biol. 4, 174. https://doi.org/10.1038/msb.2008.10.

Dragosits, M., Mattanovich, D., 2013. Adaptive laboratory evolution – principles and applications for biotechnology. Microb. Cell Factories 12, 64. https://doi.org/10.1186/1475-2859-12-64.

Elliott, K.T., Cuff, L.E., Neidle, E.L., 2013. Copy number change: evolving views on gene amplification. Future Microbiol. 8, 887–899. https://doi.org/10.2217/fmb.13.53.

Espah Borujeni, A., Channarasappa, A.S., Salis, H.M., 2014. Translation rate is controlled by coupled trade-offs between site accessibility, selective RNA unfolding and sliding at upstream standby sites. Nucleic Acids Res. 42, 2646–2659. https://doi.org/10.1093/nar/gkt1139.

Fischer, R., Bleichrodt, F.S., Gerischer, U., 2008. Aromatic degradative pathways in *Acinetobacter baylyi* underlie carbon catabolite repression. Microbiology 154, 3095–3103. https://doi.org/10.1099/mic.0.2008/016907-0.

Franden, M.A., Jayakody, L.N., Li, W.J., Wagner, N.J., Cleveland, N.S., Michener, W.E., Hauer, B., Blank, L.M., Wierckx, N., Klebensberger, J., Beckham, G.T., 2018. Engineering *Pseudomonas putida* KT2440 for efficient ethylene glycol utilization. Metab. Eng. 48, 197–207. https://doi.org/10.1016/j.ymben.2018.06.003.

Fuchs, G., Boll, M., Heider, J., 2011. Microbial degradation of aromatic compounds — from one strategy to four. Nat. Rev. Microbiol. 9, 803–816. https://doi.org/10.1038/nrmicro2652.

Garcia, J.M., Robertson, M.L., 2017. The future of plastics recycling. Science 84 358, 870–872. https://doi.org/10.1126/science.aaq0324.

Genee, H.J., Bali, A.P., Petersen, S.D., Siedler, S., Bonde, M.T., Gronenberg, L.S., Kristensen, M., Harrison, S.J., Sommer, M.O.A., 2016. Functional mining of transporters using synthetic selections. Nat. Chem. Biol. 12, 1015–1022. https://doi.org/10.1038/nchembio.2189.

Guzmán, G.I., Sandberg, T.E., LaCroix, R.A., Nyerges, Á., Papp, H., de Raad, M., King, Z. A., Hefner, Y., Northen, T.R., Notebaart, R.A., Pál, C., Palsson, B., Papp, B., Feist, A. M., 2019. Enzyme promiscuity shapes adaptation to novel growth substrates. Mol. Syst. Biol. 15, 1–14. https://doi.org/10.15252/msb.20188462.

Han, X., Liu, W., Huang, J.-W., Ma, J., Zheng, Y., Ko, T.-P., Xu, L., Cheng, Y.-S., Chen, C.-C., Guo, R.-T., 2017. Structural insight into catalytic mechanism of PET hydrolase. Nat. Commun. 8, 2106. https://doi.org/10.1038/s41467-017-02255-z.

Hara, H., Eltis, L.D., Davies, J.E., Mohn, W.W., 2007. Transcriptomic analysis reveals a bifurcated terephthalate degradation pathway in *Rhodococcus* sp. strain RHA1. J. Bacteriol. 189, 1641–1647. https://doi.org/10.1128/JB.01322-06.

Herrero Acero, E., Ribitsch, D., Steinkellner, G., Gruber, K., Greimel, K., Eiteljoerg, I., Trotscha, E., Wei, R., Zimmermann, W., Zinn, M., Cavaco-Paulo, A., Freddi, G., Schwab, H., Guebitz, G., 2011. Enzymatic surface hydrolysis of PET: effect of structural diversity on kinetic properties of cutinases from *Thermobifida*. Macromolecules 44, 4632–4640. https://doi.org/10.1021/ma200949p.

Herrou, J., Czyz, D.M., Fiebig, A., Willett, J.W., Kim, Y., Wu, R., Babnigg, G., Crosson, S., 2018. Molecular control of gene expression by *Brucella* BaaR, an IclR-type transcriptional repressor. J. Biol. Chem. 293, 7437–7456. https://doi.org/10.1074/jbc.RA118.002045.

Hosaka, M., Kamimura, N., Toribami, S., Mori, K., Kasai, D., Fukuda, M., Masai, E., 2013. Novel tripartite aromatic acid transporter essential for terephthalate uptake in *Comamonas* sp. strain E6. Appl. Environ. Microbiol. 79, 6148–6155. https://doi.org/10.1128/AEM.01600-13.

IHS Markit, 2019. Chemical Economics Handbook: CEH: Dimethyl Terephthalate (DMT) & Terephthalic Acid (TPA).

Jha, R.K., Bingen, J.M., Johnson, C.W., Kern, T.L., Khanna, P., Trettel, D.S., Strauss, C.E. M., Beckham, G.T., Dale, T., 2018. A protocatechuate biosensor for *Pseudomonas putida* KT2440 via promoter and protein evolution. Metab. Eng. Commun. 6, 33–38. https://doi.org/10.1016/j.meteno.2018.03.001.

Jha, R.K., Kern, T.L., Fox, D.T., Strauss, M., C, E., 2014. Engineering an *Acinetobacter* regulon for biosensing and high-throughput enzyme screening in *E. coli* via flow cytometry. Nucleic Acids Res. 42, 8150–8160. https://doi.org/10.1093/nar/gku444.

Johnson, C.W., Beckham, G.T., 2015. Aromatic catabolic pathway selection for optimal production of pyruvate and lactate from lignin. Metab. Eng. 28, 240–247. https://doi.org/10.1016/j.ymben.2015.01.005.

Johnson, C.W., Salvachúa, D., Rorrer, N.A., Black, B.A., Vardon, D.R., St John, P.C., Cleveland, N.S., Dominick, G., Elmore, J.R., Grundl, N., Khanna, P., Martinez, C.R., Michener, W.E., Peterson, D.J., Ramirez, K.J., Singh, P., VanderWall, T.A., Wilson, A. N., Yi, X., Biddy, M.J., Bomble, Y.J., Guss, A.M., Beckham, G.T., 2019. Innovative chemicals and materials from bacterial aromatic catabolic pathways. Joule 3, 1523–1537. https://doi.org/10.1016/j.joule.2019.05.011.

Joo, S., Cho, I.J., Seo, H., Son, H.F., Sagong, H.-Y., Shin, T.J., Choi, S.Y., Lee, S.Y., Kim, K.-J., 2018. Structural insight into molecular mechanism of poly(ethylene terephthalate) degradation. Nat. Commun. 9, 382. https://doi.org/10.1038/s41467-018-02881-1.

Kasai, D., Kitajima, M., Fukuda, M., Masai, E., 2010. Transcriptional regulation of the terephthalate catabolism operon in *Comamonas* sp. strain E6. Appl. Environ. Microbiol. 76, 6047–6055. https://doi.org/10.1128/AEM.00742-10.

Kenny, S.T., Runic, J.N., Kaminsky, W., Woods, T., Babu, R.P., Keely, C.M., Blau, W., O'Connor, K.E., 2008. Up-cycling of PET (polyethylene terephthalate) to the biodegradable plastic PHA (polyhydroxyalkanoate). Environ. Sci. Technol. 42, 7696–7701. https://doi.org/10.1021/es801010e.

Kenny, S.T., Runic, J.N., Kaminsky, W., Woods, T., Babu, R.P., O'Connor, K.E., 2012. Development of a bioprocess to convert PET derived terephthalic acid and biodiesel derived glycerol to medium chain length polyhydroxyalkanoate. Appl. Microbiol. Biotechnol. 95, 623–633. https://doi.org/10.1007/s00253-012-4058-4.

Li, W.J., Jayakody, L.N., Franden, M.A., Wehrmann, M., Daun, T., Hauer, B., Blank, L.M., Beckham, G.T., Klebensberger, J., Wierckx, N., 2019. Laboratory evolution reveals the metabolic and regulatory basis of ethylene glycol metabolism by *Pseudomonas putida* KT2440. Environ. Microbiol. 21, 3669–3682. https://doi.org/10.1111/1462-2920.14703.

Linger, J.G., Vardon, D.R., Guarnieri, M.T., Karp, E.M., Hunsinger, G.B., Franden, M.A., Johnson, C.W., Chupka, G., Strathmann, T.J., Pienkos, P.T., Beckham, G.T., 2014. Lignin valorization through integrated biological funneling and chemical catalysis. Proc. Natl. Acad. Sci. 111, 12013–12018. https://doi.org/10.1073/pnas.1410657111.

Livak, K.J., Schmittgen, T.D., 2001. Analysis of relative gene expression data using real-time quantitative PCR and the $2^{-\Delta\Delta Ct}$ method. Methods 25, 402–408. https://doi.org/10.1006/meth.2001.1262.

Luo, Z.W., Lee, S.Y., 2017. Biotransformation of *p*-xylene into terephthalic acid by engineered *Escherichia coli*. Nat. Commun. 8, 15689. https://doi.org/10.1038/ncomms15689.

McLeod, M.P., Warren, R.L., Hsiao, W.W.L., Araki, N., Myhre, M., Fernandes, C., Miyazawa, D., Wong, W., Lillquist, A.L., Wang, D., Dosanjh, M., Hara, H., Petrescu, A., Morin, R.D., Yang, G., Stott, J.M., Schein, J.E., Shin, H., Smailus, D., Siddiqui, A.S., Marra, M.A., Jones, S.J.M., Holt, R., Brinkman, F.S.L., Miyauchi, K., Fukuda, M., Davies, J.E., Mohn, W.W., Eltis, L.D., 2006. The complete genome of *Rhodococcus* sp. RHA1 provides insights into a catabolic powerhouse. Proc. Natl. Acad. Sci. 103, 15582–15587. https://doi.org/10.1073/pnas.0607048103.

Metzgar, D., Bacher, J.M., Pezo, V., Reader, J., Doring, V., Schimmel, P., Marliere, P., Crecy-Lagard, V., 2004. *Acinetobacter* sp. ADP1: an ideal model organism for genetic analysis and genome engineering. Nucleic Acids Res. 32, 5780–5790. https://doi.org/10.1093/nar/gkh881.

Mückschel, B., Simon, O., Klebensberger, J., Graf, N., Rosche, B., Altenbuchner, J., Pfannstiel, J., Huber, A., Hauer, B., 2012. Ethylene glycol metabolism by *Pseudomonas putida*. Appl. Environ. Microbiol. 78, 8531–8539. https://doi.org/10.1128/AEM.02062-12.

Müller, R.-J., Schrader, H., Profe, J., Dresler, K., Deckwer, W.-D., 2005. Enzymatic degradation of poly(ethylene terephthalate): rapid hydrolyse using a hydrolase from *T. fusca*. Macromol. Rapid Commun. 26, 1400–1405. https://doi.org/10.1002/marc.200500410.

NAPCOR (National Association for PET Container), 2018. Report on Postconsumer PET Container Recycling Activity in 2017.

Palm, G.J., Reisky, L., Böttcher, D., Müller, H., Michels, E.A.P., Walczak, M.C., Berndt, L., Weiss, M.S., Bornscheuer, U.T., Weber, G., 2019. Structure of the plastic-degrading *Ideonella sakaiensis* MHETase bound to a substrate. Nat. Commun. 10, 1–10. https://doi.org/10.1038/s41467-019-09326-3.

Parke, D., Garcia, M. a, Ornston, L.N., 2001. Cloning and genetic characterization of *dca* genes required for oxidation of straight-chain dicarboxylic acids in *Acinetobacter* sp. strain ADP1. Appl. Environ. Microbiol. 67, 4817–4827. https://doi.org/10.1128/AEM.67.10.4817-4827.2001.

Patrauchan, M.A., Florizone, C., Dosanjh, M., Mohn, W.W., Davies, J., Eltis, L.D., 2005. Catabolism of benzoate and phthalate in *Rhodococcus* sp. strain RHA1: redundancies and convergence. J. Bacteriol. 187, 4050–4063. https://doi.org/10.1128/JB.187.12.4050-4063.2005.

Pédelacq, J.-D., Cabantous, S., Tran, T., Terwilliger, T.C., Waldo, G.S., 2006. Engineering and characterization of a superfolder green fluorescent protein. Nat. Biotechnol. 24, 79–88. https://doi.org/10.1038/nbt1172.

Portnoy, V.A., Bezdan, D., Zengler, K., 2011. Adaptive laboratory evolution—harnessing the power of biology for metabolic engineering. Curr. Opin. Biotechnol. 22, 590–594. https://doi.org/10.1016/j.copbio.2011.03.007.

Rahimi, A., García, J.M., 2017. Chemical recycling of waste plastics for new materials production. Nat. Rev. Chem. 1, 46. https://doi.org/10.1038/s41570-017-0046.

Renda, B.A., Dasgupta, A., Leon, D., Barrick, J.E., 2015. Genome instability mediates the loss of key traits by *Acinetobacter baylyi* ADP1 during laboratory evolution. J. Bacteriol. 197, 872–881. https://doi.org/10.1128/JB.02263-14.

Ribitsch, D., Acero, E.H., Greimel, K., Eiteljoerg, I., Trotscha, E., Freddi, G., Schwab, H., Guebitz, G.M., 2012. Characterization of a new cutinase from *Thermobifida alba* for PET-surface hydrolysis. Biocatal. Biotransform. 30, 2–9. https://doi.org/10.3109/10242422.2012.644435.

Rogers, J.K., Church, G.M., 2016. Genetically encoded sensors enable real-time observation of metabolite production. Proc. Natl. Acad. Sci. 113, 2388–2393. https://doi.org/10.1073/pnas.1600375113.

Ronkvist, Å.M., Xie, W., Lu, W., Gross, R.A., 2009. Cutinase-catalyzed hydrolysis of poly (ethylene terephthalate). Macromolecules 42, 5128–5138. https://doi.org/10.1021/ma9005318.

Rorrer, N.A., Nicholson, S., Carpenter, A., Biddy, M.J., Grundl, N.J., Beckham, G.T., 2019. Combining reclaimed PET with bio-based monomers enables plastics upcycling. Joule 3, 1006–1027. https://doi.org/10.1016/j.joule.2019.01.018.

Salis, H.M., Mirsky, E.A., Voigt, C.A., 2009. Automated design of synthetic ribosome binding sites to control protein expression. Nat. Biotechnol. 27, 946–950. https://doi.org/10.1038/nbt.1568.

Salvador, M., Abdulmutalib, U., Gonzalez, J., Kim, J., Smith, A.A., Faulon, J.-L., Wei, R., Zimmermann, W., Jimenez, J.I., 2019. Microbial genes for a circular and sustainable bio-PET economy. Genes (Basel). 10, 373. https://doi.org/10.3390/genes10050373.

Sandberg, T.E., Salazar, M.J., Weng, L.L., Palsson, B., Feist, A.M., 2019. The emergence of adaptive laboratory evolution as an efficient tool for biological discovery and industrial biotechnology. Metab. Eng. 56, 1–16. https://doi.org/10.1016/j.ymben.2019.08.004.

Sasoh, M., Masai, E., Ishibashi, S., Hara, H., Kamimura, N., Miyauchi, K., Fukuda, M., 2006. Characterization of the terephthalate degradation genes of *Comamonas* sp. strain E6. Appl. Environ. Microbiol. 72, 1825–1832. https://doi.org/10.1128/AEM.72.3.1825.

Schmidt-Rose, T., Jentsch, T.J., 1997. Reconstitution of functional voltage-gated chloride channels from complementary fragments of CLC-1. J. Biol. Chem. 272, 20515–20521. https://doi.org/10.1074/jbc.272.33.20515.

Seaton, S.C., Elliott, K.T., Cuff, L.E., Laniohan, N.S., Patel, P.R., Neidle, E.L., 2012. Genome-wide selection for increased copy number in *Acinetobacter baylyi* ADP1: locus and context-dependent variation in gene amplification. Mol. Microbiol. 83, 520–535. https://doi.org/10.1111/j.1365-2958.2011.07945.x.

Shanley, M.S., Neidle, E.L., Parales, R.E., Ornston, L.N., 1986. Cloning and expression of *Acinetobacter calcoaceticus catBCDE* genes in *Pseudomonas putida* and *Escherichia coli*. J. Bacteriol. 165, 557–563. https://doi.org/10.1128/JB.165.2.557-563.1986.

Shigematsu, T., Yumihara, K., Ueda, Y., Morimura, S., Kida, K., 2003. Purification and gene cloning of the oxygenase component of the terephthalate 1,2-dioxygenase system from *Delftia tsuruhatensis* strain T7. FEMS Microbiol. Lett. 220, 255–260. https://doi.org/10.1016/S0378-1097(03)00124-1.

Siehler, S.Y., Dal, S., Fischer, R., Patz, P., Gerischer, U., 2007. Multiple-level regulation of genes for protocatechuate degradation in *Acinetobacter baylyi* includes cross-regulation. Appl. Environ. Microbiol. 73, 232–242. https://doi.org/10.1128/AEM.01608-06.

Sinha, V., Patel, M.R., Patel, J.V., 2010. PET waste management by chemical recycling: a review. J. Polym. Environ. 18, 8–25. https://doi.org/10.1007/s10924-008-0106-7.

Suárez, G.A., Renda, B.A., Dasgupta, A., Barrick, J.E., 2017. Reduced mutation rate and increased transformability of transposon-free *Acinetobacter baylyi* ADP1-ISx. Appl. Environ. Microbiol. 83, 17. https://doi.org/10.1128/AEM.01025-17.

Sulaiman, S., Yamato, S., Kanaya, E., Kim, J.J., Koga, Y., Takano, K., Kanaya, S., 2012. Isolation of a novel cutinase homolog with polyethylene terephthalate-degrading activity from leaf-branch compost by using a metagenomic approach. Appl. Environ. Microbiol. 78, 1556–1562. https://doi.org/10.1128/AEM.06725-11.

Tomanek, I., Grah, R., Lagator, M., Andersson, A.M.C., Bollback, J.P., Tkačik, G., Guet, C. C., 2020. Gene amplification as a form of population-level gene expression regulation. Nat. Ecol. Evol. https://doi.org/10.1038/s41559-020-1132-7.

Tumen-Velasquez, M., Johnson, C.W., Ahmed, A., Dominick, G., Fulk, E.M., Khanna, P., Lee, S.A., Schmidt, A.L., Linger, J.G., Eiteman, M.A., Beckham, G.T., Neidle, E.L., 2018. Accelerating pathway evolution by increasing the gene dosage of chromosomal segments. Proc. Natl. Acad. Sci. 115, 7105–7110. https://doi.org/10.1073/pnas.1803745115.

Vermaas, J.V., Dixon, R.A., Chen, F., Mansfield, S.D., Boerjan, W., Ralph, J., Crowley, M. F., Beckham, G.T., 2019. Passive membrane transport of lignin-related compounds.

Proc. Natl. Acad. Sci. 116, 23117–23123. https://doi.org/10.1073/pnas.1904643116.

Wang, Y.Z., Zhou, Y., Zylstra, G.J., 1995. Molecular analysis of isophthalate and terephthalate degradation by *Comamonas testosteroni* YZW-D. Environ. Health Perspect. 103, 9–12. https://doi.org/10.2307/3432469.

Wierckx, N., Prieto, M.A., Pomposiello, P., de Lorenzo, V., O'Connor, K., Blank, L.M., 2015. Plastic waste as a novel substrate for industrial biotechnology. Microb. Biotechnol. 8, 900–903. https://doi.org/10.1111/1751-7915.12312.

Williams, P.A., Shaw, L.E., 1997. mucK, a gene in *Acinetobacter calcoaceticus* ADP1 (BD413), encodes the ability to grow on exogenous *cis,cis*-muconate as the sole carbon source. J. Bacteriol. 179, 5935–5942. https://doi.org/10.1128/JB.179.18.5935-5942.1997.

Winnen, B., Hvorup, R.N., Saier, M.H., 2003. The tripartite tricarboxylate transporter (TTT) family. Res. Microbiol. 154, 457–465. https://doi.org/10.1016/S0923-2508(03)00126-8.

Yoshida, S., Hiraga, K., Takehana, T., Taniguchi, I., Yamaji, H., Maeda, Y., Toyohara, K., Miyamoto, K., Kimura, Y., Oda, K., 2016. A bacterium that degrades and assimilates poly(ethylene terephthalate). Science 80, 1196–1199. https://doi.org/10.1126/science.aad6359.

Young, D.M., Parke, D., Ornston, L.N., 2005. Opportunities for genetic investigation afforded by *Acinetobacter baylyi*, a nutritionally versatile bacterial species that is highly competent for natural transformation. Annu. Rev. Microbiol. 59, 519–551. https://doi.org/10.1146/annurev.micro.59.051905.105823.

Zen, K.H., McKenna, E., Bibi, E., Hardy, D., Kaback, H.R., 1994. Expression of lactose permease in contiguous fragments as a probe for membrane-spanning domains. Biochemistry 33, 8198–8206. https://doi.org/10.1021/bi00193a005.

Zhang, J., Jensen, M.K., Keasling, J.D., 2015. Development of biosensors and their application in metabolic engineering. Curr. Opin. Chem. Biol. 28, 1–8. https://doi.org/10.1016/j.cbpa.2015.05.013.